

See discussions, stats, and author profiles for this publication at: <https://www.researchgate.net/publication/384320045>

Predictive modelling of pharmaceutical powder formulations: finite element simulations of the compaction of elastic/plastic binary mixtures

Thesis · August 2021

DOI: 10.13140/RG.2.2.30309.00489

CITATIONS

0

READS

30

1 author:



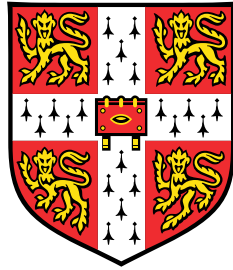
Danny van der Haven

ETH Zurich

17 PUBLICATIONS 34 CITATIONS

SEE PROFILE

Predictive modelling of pharmaceutical powder formulations: finite element simulations of the compaction of elastic/plastic binary mixtures



Dingeman L.H. van der Haven

Academic supervisor: Prof. J.A. Elliott

Industrial supervisor: Dr. I.S. Fragkopoulos

Department of Physics
University of Cambridge

This dissertation is submitted for the degree of
Master of Philosophy

Hughes Hall

August 2021

Declaration

This Dissertation is substantially my own work and conforms to the University of Cambridge's guidelines on plagiarism. Where reference has been made to other research this is acknowledged in the text and bibliography.

Dingeman L.H. van der Haven
August 2021

Acknowledgements

I would like to express my sincere gratitude towards Prof. James Elliott (University of Cambridge, Macromolecular Materials Laboratory) and Dr. Ioannis Fragkopoulos (Novo Nordisk, Oral Protein Formulation) for their continued guidance. Their regular feedback has strongly improved the quality of this report and motivated me to make the most out of this project.

This MPhil project has been financed by Novo Nordisk A/S (Bagsværd, Denmark). I would therefore like to thank Novo Nordisk for granting me this opportunity. In particular I also want to thank the following people at Novo Nordisk: Dr. Kaisa Naelapää (Oral Formulation Research) as industrial co-supervisor, Frederik Ørtoft (Oral Formulation Research) for the compaction experiments, and Karolina Wszola (Oral Protein Formulation) for the crushing experiments and discussions about FEM simulations.

Abstract

A numerical method, which only uses single-component experimental data, was developed to predict the compaction behaviour of pharmaceutical powder mixtures. Material properties of single-component powders were described using the density-dependent Drucker-Prager Cap (dDPC) model. Mixing rules for the material properties were defined by applying the isostress condition within the material. Hereafter, the mixing rules were used to obtain the elastic and dDPC model parameters for various powder mixtures. These model parametrisations were implemented into a Finite Element Method (FEM) calculation using the commercial code Abaqus 2019 with a user-defined subroutine. Mixtures of micro-crystalline cellulose (MCC, plastic) and dibasic calcium phosphate dihydrate (DCPD, brittle) powders were used to validate the parametrisations and the mixing rules. Parametrisations of the dDPC model were extracted from experimental data using an automated work-flow that is robust and requires minimal user input. FEM simulations that used parametrisations derived directly from experimental data predicted the experimental compaction curves with a mean error of 2.5% of the maximum compaction pressure. Parametrisations derived using mixing rules resulted in predictions for powder mixtures with a mean error of 4.8%. Furthermore, stress profiles displayed the same trend with respect to the composition of the tablet, regardless of the parametrisation method. This numerical methodology can thus be used to predict the compaction behaviour of binary powder mixtures without the need for any experimental data except that of the single-component powders. Furthermore, the method may readily be extended towards an arbitrary number of components to further accelerate the identification of pharmaceutical powder mixtures that result in tablets with high structural integrity.

Table of contents

1	Introduction	1
1.1	Introduction	1
2	Literature review	3
2.1	The Drucker-Prager cap (DPC) model for compaction of pharmaceutical powders	4
2.1.1	Model introduction and initial validation studies	4
2.1.2	Extension to density-dependent material properties	4
2.1.3	Studies on variations in punch geometry and friction	4
2.1.4	Application in 3D crushing simulations	5
2.2	Improvements of the density-dependent DPC model	6
2.2.1	Parameter sensitivity studies	6
2.2.2	Parameter extrapolations	7
2.2.3	Visco-elastic behaviour	8
2.3	Predicting compacted properties of powder mixtures	8
3	Experiment set-up and preprocessing	11
3.1	Choice of tablet materials	11
3.2	Uniaxial tablet compaction	11
3.3	Automated preprocessing	14
3.4	Extension of compaction curves	15
3.5	Quantitative comparison of compaction curves	16
3.6	Die wall friction	17
3.7	True densities	19
3.8	Tensile strengths from crushing experiments	20
4	Defining material properties (direct parametrisation)	23
4.1	Density-dependent Drucker-Prager Cap (dDPC) model	23

4.2	Cohesion and internal friction angle	25
4.3	Elastic parameters	26
4.4	Relative density	29
4.5	Plastic parameters	30
4.6	Fitting and extrapolating the DPC parameters	32
5	Estimation of mixture properties (indirect parametrisation)	35
5.1	True density and volume fraction	35
5.2	Reynolds et al. model	36
5.3	Layered or (microscopically-)segregated tablets	36
5.4	Mixing rules	38
6	FEM and numerical modelling details	41
6.1	Geometry and meshing	41
6.2	Numerical integration	43
6.3	Powder properties and subroutine	44
6.4	Output	44
7	Results and discussion	47
7.1	Direct parametrisation	47
7.1.1	Validation of the direct method	47
7.1.2	Qualitative identification of tablet defects	53
7.1.3	Evaluation of crushing simulations	54
7.2	Indirect parametrisation (layered)	56
7.2.1	Validation of the indirect layered method	56
7.2.2	Implications for the mixing model	58
7.2.3	The effect of layer arrangement on the radial stress	59
7.3	Indirect parametrisation (mixed)	60
8	Conclusions and outlook	63
8.1	Conclusion	63
8.2	Outlook	64
	References	67

Chapter 1

Introduction

1.1 Introduction

The tablet is the most popular dosage form within the pharmaceutical industry. This popularity stems from the many advantages of tablets, such as physical and chemical stability, dosage precision, easy large-scale production, and patient-friendliness. However, not all pharmaceutical compounds can easily be made into tablets. Tablet defects such as capping, lamination, or chipping can occur (Fig. 1.1). Tablets can also be too porous or too dense, causing either accelerated or poor release of the active pharmaceutical ingredients (APIs). Defective tablets are costly because of production delays or product recalls. It is therefore of major interest to try and prevent these tableting defects.

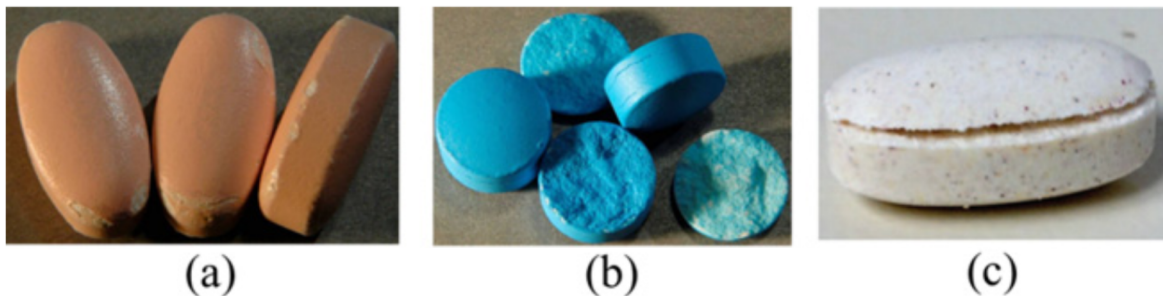


Fig. 1.1 Common defects in tablets: (a) chipping, (b) lamination, and (c) capping. Figure taken from Baroutaji et al.[1]

The frequency of tableting defects depends strongly on the formulation and production process. The most common production method is direct compression. The APIs are formulated into a powder together with other components, such as excipients or colourings. The powder is then compacted using a tableting press. A die is filled with the powder and two

punches are used to compact the powder into a tablet. Even for a single formulation, variations in compaction pressure, compaction speed, and punch shape can affect the structural integrity of the tablet. Because of the large number of tuning parameters, experimental trial and error is a costly undertaking. This has made computational methods increasingly popular for troubleshooting and design of the tableting process.

Although the powders are granular materials, typically containing particles with a size of tens to hundreds of micrometers, continuum models have already been successful in predicting potential tablet defects. A finite-element method (FEM) can thus be used to simulate the entire compaction process on a full-sized scale and help the design of the tableting process. To do so, FEM models need to have an accurate representation of all material properties. The mechanical behaviour of the powder is thus typically defined using an elasto-plastic constitutive model, such as the density-dependent Drucker-Prager cap (dDPC), crushable foam, or modified Cam-Clay model. Experimental data can then be used to parametrise the model and indeed get a FEM model that closely mimics experimental results. It is this approach, in particular with the dDPC model, that has had success in predicting the compaction curve, defects, and even the tensile strength of tablets.

Studies in the past have considered either pure excipients or a specific powder formulation or mixture. The current approach therefore requires experimental data, and sometimes *ad hoc* fitting procedures, for each and every mixture. Nonetheless, a wide range of powder mixtures may be considered during the development process, in particular mixtures in which the ratio of two components is changed. Parametrising the dDPC model with experimental data of each and every mixture becomes infeasible because this requires large quantities of experimental data. It is thus most desirable to have a method that only uses single-component material parameters to predict the behaviour of powder mixtures.

The aim of this thesis is to develop a method to i) parametrise the dDPC model for FEM simulations of pure materials in an automated manner and ii) use single-material parametrisations to predict the dDPC model parameters, and thus the compaction behaviour, of powder mixtures.

Chapter 2 provides a literature review the application of FEM to pharmaceutical powders. Particularly, developments with respect to the dDPC model and extension thereof are considered. Chapter 3 describes the experimental methods. Chapter 4 explains how the experimental data was used to parametrise the dDPC model. Chapter 5 then extends the parametrisation to describe the compaction behaviour of powder mixtures using only single-component experimental data. Chapter 6 describes the FEM simulations of the powder compaction process. Chapter 7 discusses the results of the simulations and compares these to experiment. Finally, the conclusion and outlook are given in chapter 8.

Chapter 2

Literature review

The aim of this chapter is to summarise literature on FEM simulations of uniaxial compaction and provide a suitable starting point for developing a framework to predict powder-mixture behaviour. A proper parametrisation of the powder's material properties is vital for any FEM framework regarding powder compaction. Although the modified Cam-Clay model is also used regularly, the Drucker-Prager cap (DPC) model is by far the most widely used model for describing the properties of pharmaceutical powders in FEM simulations. It is one of the few models that only needs a limited number of experiments to fully define the behaviour of a granular material and gives a reasonable accuracy. For these reasons, the DPC model with its developments and applications are discussed in detail. The last part of this review presents an overview of the current methods for predicting mixture properties.

This review limits itself to the discussion of uniaxial compaction and crushing of tablets. Roll compaction is another popular method within the pharmaceutical industry but is discussed elsewhere.[2–6] All but one of the studies used the commercial Abaqus software (Dassault Systèmes, Vélizy-Villacoublay, France) to do FEM simulations of powder compaction.[7] The other study used Ansys (Ansys Inc., Canonsburg, USA) instead. [8, 9] Furthermore, all studies assumed radial symmetry with tablets represented as a 2D slice by using axisymmetric elements. The parametrisation methodology itself is typically discussed within the methods section of the papers but can also be found in dedicated papers.[10, 11]

2.1 The Drucker-Prager cap (DPC) model for compaction of pharmaceutical powders

2.1.1 Model introduction and initial validation studies

The first published use of the DPC model to simulate powder compaction was by Michrafy et al. (2002,2003,2004).[12–14] Their FEM simulations gave predictions for the stress and density profiles within the tablet. This provided an initial tool for the identification of potential tablet defects. For example, Michrafy et al. predicted that capping may occur in lactose tablets because of the presence of stress bands going from the centre to the tip of the tablet. Wu et al. (2005) subsequently repeated their studies in greater detail, also simulating lactose tablets, and confirmed their predictions.[15] Experimentally produced lactose tablets indeed showed capping and X-ray computed tomography experiments confirmed crack development along the predicted stress bands. The potential of the DPC model to assist in the tableting process development was therefore immediately demonstrated, especially given that these parametrisations of the DPC model used only uniaxial compaction data.

2.1.2 Extension to density-dependent material properties

The original DPC model still had the predominant shortcoming that material properties did not depend on the density of the powder. This shortcoming was also hypothesised to be responsible for the excessive elastic recovery of some simulated tablets.[12, 16] The density-dependent DPC (dDPC) model was first implemented by Sinka et al. (2003) and seemed to improve density predictions.[17] A comparative study by Sinha et al. (2010) later confirmed that the dDPC indeed gives more accurate predictions for the density profile.[18]

2.1.3 Studies on variations in punch geometry and friction

Sinka et al. (2003) demonstrated and experimentally confirmed that friction was shown to have a pronounced effect on the final density distribution of the tablets. The trend between friction and the density distribution inverts at some point. Conclusions regarding the effect of friction could therefore not be generalised.

Wu et al. (2008) followed up on their previous studies in 2005 and studied lactose tablets again using the DPC model while considering variations in friction, punch geometry, compaction profile, compaction speed, and final thickness of the tablet.[19] However, none of the considered variations were able to completely avoid the development of intense stress

bands and thereby avoid potential capping. This already implied that models would eventually have to be expanded to consider changes in the powder composition as well.

Han et al. (2008) performed a study similar to Wu et al. (2005) but with the dDPC model and micro-crystalline cellulose (MCC).[20, 21] In all cases, large stresses were observed near the edge of the tablet upon ejection, caused by the radial elastic recovery of the tablet. Furthermore, the observed stress and density distributions supported the experimental observation that concave tablets show more capping but less chipping than flat-faced tablets. Kadiri and Michrafy (2013) did a similar study and found that capping tendency indeed increases as the radius of curvature decreases.[22] However, a relatively high friction coefficient of 0.4 was used and the trend may not hold for lower friction coefficients. An extensive study on the effects of friction and punch geometry by Krok et al. (2014) confirmed this.[23] Using punches that are more concave or increasing the friction resulted in increased densities near the die wall. But the optimum punch shape depends on the friction and material. The absence of a general trend leads to the conclusion that case-by-case considerations are necessary when trying to prevent capping.

Several lower punches with protrusions (cylindrical, hemispherical, and conical) were also investigated by Han et al. (2011).[24] Density and stress distributions were in qualitative agreement with X-ray computed tomography and 2D-SAXS data. Moreover, discolouration of some tablets at high-density regions suggested scorching due to internal dissipation by granule deformation or friction, suggesting that modelling thermo-mechanical behaviour may also help predicting defects.

2.1.4 Application in 3D crushing simulations

Krok et al. (2014) tested the validity of representing 3D tablets with 2D axisymmetric slices and found that the error in compaction pressure was less than 1%.[23] Nonetheless, a number of studies did consider 3D tablets because of tablet geometries or numerical experiments without radial symmetry. The first was Klinzing et al. (2010), who considered the uniaxial compaction of capsule-shaped tablets of MCC.[25] Predicted density distributions were in good agreement with X-ray computed tomography experiments. This underlines that both 2D and 3D representations using the dDPC model are valid.

Shang et al. (2x 2013) used the dDPC model in 3D to study the diametrical crushing of tablets with different shapes.[26, 27] Various failure criteria were compared assuming a tablet of uniform density. A maximum principal stress on the diameter that exceeds the material tensile strength was found to be the most reliable failure criterion. X-ray computed tomography showed that the failure patterns predicted using this criterion corresponded with experimental failure patterns. These studies proposed that these methods can be used to

replace empirical equations when predicting the breaking force for tablet with more complex shapes.

Furukawa et al. (2015) improved on the aforementioned studies.[28] To account for density variations within the tablet, the compaction process was simulated before simulating a diametrical crushing test. After ejection, two plates were used to crush the tablet. Active yielding (Abaqus option AC YIELD) of the mesh elements was then used to track the development of failure zones. When yielding started near the centre of the tablet this resulted in capping or lamination, whereas yielding near the periphery resulted only in a crack in the direction of force. Experimental high-speed camera observations confirmed the predicted failure patterns. These studies show that the dDPC model also has the potential to predict the exact point of failure instead of only qualitative comparisons.

2.2 Improvements of the density-dependent DPC model

2.2.1 Parameter sensitivity studies

Despite the aforementioned successes, a number of shortcomings of the DPC model have also come to light, together with various attempts to compensate for them. Sinha et al. (2010) performed a sensitivity study on the DPC model parametrisation for lactose and micro-crystalline cellulose (MCC) by varying the cohesion and friction angle.[16] During decompression, extreme dilation of the tablet and poor convergence were observed for low cohesions (≤ 0.1 MPa) or moderate cohesion (1 MPa) with low friction angles ($\leq 45^\circ$). It was concluded that the dilation and convergence issues are caused by improper parametrisation of the cohesion and friction angle, which cause excessive shear yielding of the tablet during recovery. Moreover, some tablets do not show shear failure during the compaction process, which makes it impossible to determine the cohesion and friction angle with only uniaxial compaction experiments. The introduction of tensile strength (or crushing) experiments to define the shear failure line by Sinka et al. (2003) addressed these concerns.[17] Another concern was expressed by studies by Mazel et al. (2x 2014) who used FEM and tensile strength experiments to study shear failure in tablets.[29, 30] They showed that the Drucker-Prager failure criterion is not optimally suited for describing shear failure during uniaxial compression because it underestimates the failure stress. The Drucker-Prager criterion has nonetheless remained the standard due to its practicality.

The implementation of the correct elastic behaviour of the tablets appears to be a recurring problem. The original DPC model showed excessive elastic recovery, which was subsequently resolved by implementing the dDPC model. However, even for the dDPC model problems

remain. Klinzing et al. (2010) reported that simulations overestimated the the residual stress in the tablet and attributed this to the model not capturing the nonlinear elastic recovery of the tablet.[25] Among others, Diarra et al. (2012) reported that experimental compaction curves showed a nonlinear decay of the compaction pressure whereas FEM simulation predicted a linear decay.[31] The authors concluded that nonlinear elasticity laws (i.e. a non-constant Young's modules and Poisson ratio) are needed to properly capture the pressure decay during decompression. Bilinear elastic parameters were already introduced by Han et al. (2008), one set of parameters for low pressures and one set for high pressures. [20, 21] The compaction simulations seem to display a nonlinear decay of the compaction pressure but residual pressures were not reported, making it unclear if using bilinear elastic parameters resolved both issues. The procedure by Han et al. also warrants some scepticism because the low-pressure elastic parameters are determined using the last part of the decompression stage, which is known to cause failure in some tablets. A better procedure for determining nonlinear elastic parameters may be that described by Mazel et al.[32] This procedure uses adjusted uniaxial compaction experiments and would require minimal effort if compaction curves are already being generated. However, no published study on simulating tablet compaction has implemented this procedure in their parametrisation yet.

Diarra et al. (2018) also reported a sensitivity study on the effects of changing the linear elastic parameters by $\pm 20\%$.[33] Under constant compaction pressure, changes in the Young's modulus had negligible effect on the final thickness as well as the density and stress distributions of the tablets, only the thickness during compaction shifted. Higher Poisson's ratios resulted in thicker tablets, higher axial-to-radial stress transmission, and lower residual radial stress. The radial stress distributions after decompression were strongly affected as a result of the differences in the magnitude of residual stress. This underlines the importance of properly parametrising the Poisson's ratio, as defects during decompression and ejection are often correlated with die-wall pressure.

2.2.2 Parameter extrapolations

In the study by Diarra et al. (2012), simulated compaction curves showed a considerable offset with respect to the experimental data because the parametrisation started at a higher density than the initial powder.[31] This made it evident that extrapolating the dDPC parameters to lower densities is necessary. Extrapolation of dDPC model parameters was extensively addressed by Garner et al. (2015) [34] A method was proposed for estimating dDPC model parameters outside the range of densities that can be achieved in compaction experiments. For die-compaction experiments, the low-density extrapolations had negligible effects on the compaction curves and density profiles for tablets with final relative densities above 0.6.

Nonetheless, the offset observed by Diarra et al. does demonstrate that an extrapolation is indeed necessary.[31] Furthermore, the low-density extrapolations do become important for complex geometries and roll compaction where more shearing occurs. High-density extrapolations always had a major effect on the final density profile of the tablet and must be chosen carefully. The proposed extrapolation method constrains the relative density to the physical limit of unity and seems to give satisfactory results.

2.2.3 Visco-elastic behaviour

Two experimental observations have also motivated authors to implement visco-elastic behaviour besides the dDPC model. First, the minimum tablet thickness does not always occur at the pressure maximum. And second, tablet properties depend on the compaction speed and dwell time of the punches (i.e. the delay between compression and decompression).

Diarra et al. (2013) therefore introduced creep using standard power laws for the time and strain hardening as proposed by the Abaqus software.[35] Parameters associated with these laws were determined through numerical optimization. Creep model improved the FEM results, especially during unloading, and captured the first observation mentioned. Deviations in the final part of the recovery phase indicated that other creep models may however be more suitable.

Ohsaki et al. (2020) proposed a coupling of the Peryna model to the dDPC model to include visco-plastic behaviour.[9] This allowed FEM simulations to capture the effect of punch velocity on the tableting performance. The model was parametrised using experimental data of uniaxial compaction at different velocities. They observed that a higher compression speed resulted into a higher capping frequency and less plastic deformation.

Although not related to visco-elasticity, three studies also added thermo-mechanical coupling.[36, 25, 37] Upon increasing the friction and compaction speed, the maximum temperature shifts from the centre to the top edge of the tablet. Punch shape, and thus deformation, was by far the most dominant factor determining the maximum temperature and possible tablet burn.

2.3 Predicting compacted properties of powder mixtures

The last part of this literature review aims to find a proper ansatz for a framework to predict the compaction behaviour of mixtures. The majority of studies use statistical, algorithmic, or machine-learning models to predict the mechanical properties of tablets made using powder mixtures.[38–43] Although all of these studies describe a predictive model, these models

require large quantities of experimental data to feed to non-physical models. This makes them less suitable for a bottom-up approaches or when little data is available. Preferably, the requirements on experimental data are minimized by incorporating the appropriate physics.

Queiroz et al. (2019) proposed a more physical model based on percolation theory.[44] The model is able to predict the critical fraction of API that can be put into an excipient before the excipients' mechanical properties start to change significantly, typically indicating deterioration of tableting properties. However, the model does not distinguish between differences in the final tablet density and is only defined for binary mixtures. This limits the potential for this model to help develop a generalised mixing model for dDPC parameters.

Another more physical model, based on volumetric mixing rules, was proposed by Wu et al. (2005, 2006) to predict the tensile strength of mixed-powder tablets.[45, 46] The Ryshkewitch-Duckworth equation was used to relate the tensile strength to the relative density of single-component tablets. The constants of the equation for mixtures were then predicted by weighing the pure-component constants by the volume fraction of the component in the mixture. The volume fractions were estimated using the pure-component true densities. Experimental data demonstrated the validity of the model for binary, ternary (three-components), and quaternary (four-component) mixtures of micro-crystalline cellulose, hydroxypropylmethyl cellulose, starch, and lactose monohydrate. Since the model assumes equal particle sizes, the material grades were chosen to have similar particle sizes. This hints that volumetric mixing rules might provide a promising start for mixing dDPC model parameters.

Reynolds et al. (2017) later showed that a volumetric mixing model can also be used to predict the compaction curves of mixed-powder tablets.[47] At a given stress, the compaction density of a mixture was predicted as the volumetric mean of the single-component densities. Similar to Wu et al., volume fractions were computed using the pure-component true densities and material grades were chosen to have similar particle sizes. Binary and tertiary mixtures of micro-crystalline cellulose (plastic), mannitol (intermediate), and anhydrous dicalcium phosphate (brittle) were used to validate the model. The model inherently assumes that the stress is homogeneous throughout the tablet for all materials (i.e. the isostress assumption for composites). This provides another starting point for a mixing framework.

Chapter 3

Experiment set-up and preprocessing

The first step towards simulating powder compaction is acquiring the experimental data. This chapter describes the experimental data that is needed to later parametrise the FEM model. Raw experimental data was provided by Novo Nordisk whereas all analysis on the data was done by the author.

3.1 Choice of tablet materials

The materials chosen for this study are micro-crystalline cellulose (MCC) of grade Avicel PH200 and dibasic calcium phosphate dihydrate (DCPD) of grade Emcompress premium. MCC is a typical excipient for tablet formulations and shows strongly plastic behaviour. DCPD is a material showing elastic and strongly brittle behaviour, much more akin to typical APIs.[48] Material grades were chosen to have similar particle-size distributions (see Fig. 3.1). Binary mixtures consisted of 10%-90%, 20%-80%, 50%-50% of MCC and DCPD, respectively. Mixtures were biased towards DCPD because the properties of MCC tend to dominate the behaviour of the mixture.

3.2 Uniaxial tablet compaction

Uniaxial powder compaction is the most important experiment as it closely resembles the tablet production process. These tests are needed to define the basic material properties and will be used for validation. For each mixture, tablets were produced for six to seven different final tablet densities. Ten tablets were produced for each density. The range of densities for the tablets was chosen to be as wide as possible but was limited by i) the minimum density needed to produce a cohesive tablet and ii) the radial pressure limit of the die-wall sensor.

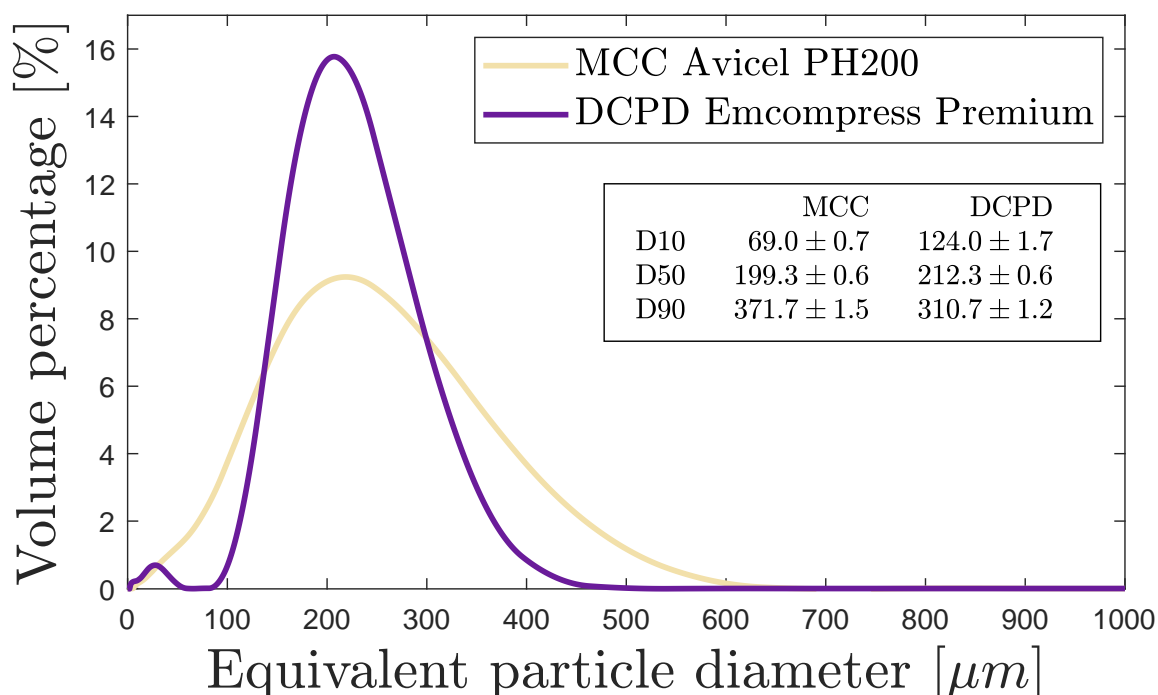


Fig. 3.1 Particle diameters resulting from laser diffraction spectroscopy using a Malvern Mastersizer 3000 (Malvern, Malvern, United Kingdom). The calculation of the diameters assumes spherical particles. The inset shows the particle sizes at 10%, 50%, and 90% of the volume of the cumulative distribution. Three experiments were done per material.

An illustration of the set-up can be seen in Fig. 3.2. Uniaxial compaction was done using the Romaco Kilian STYL'One Evolution (Medelpharm, Beynost, France) equipped with a 80 kN load cell, an instrumented cylindrical die, and circular flat-faced punches with a diameter of 11.28 mm. Before each compaction cycle, an external lubrication device was used to spray magnesium stearate onto the die and punch surfaces to ensure that the tooling was sufficiently lubricated. Powder was filled into the die using a force feeder, except for 100% MCC powder where a gravity feeder was used. The amount of powder filled into the die was also adjusted based on the target density such that the resulting thickness of the tablets was approximately equal. Hereafter, the compaction cycle begins and generally consist of three stages. The first stage is called the compression or compaction stage. The punches are brought together to consolidate the powder into a tablet. The next stage is called the unloading or decompression stage and is when the punches are moved apart again. The last stage is ejection, when the bottom punch pushes the tablet out of the die. A double-ended compaction (DEC) profile was used such that the punches moved in a V-shaped profile with a combined velocity of 0.4

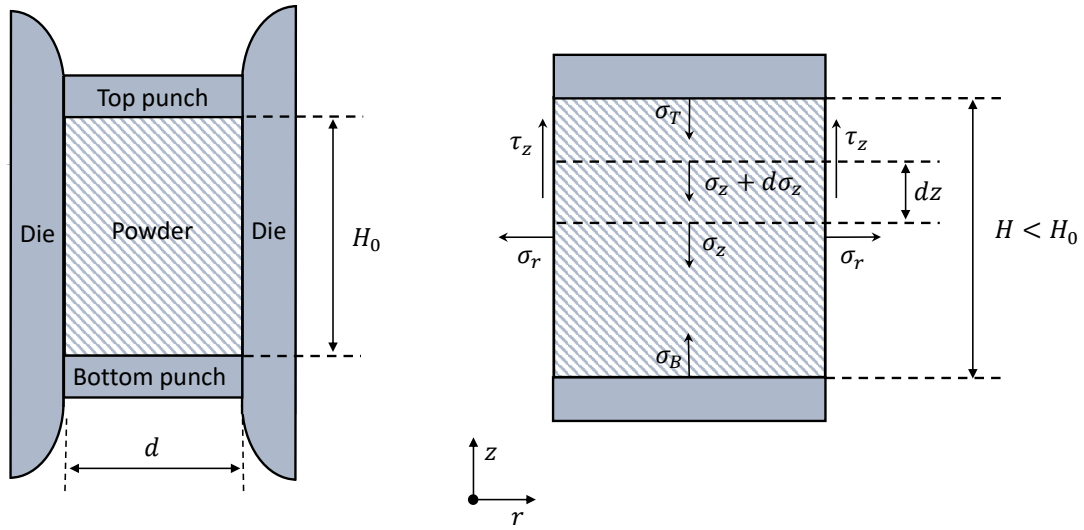


Fig. 3.2 A diagram showing the initial configuration of the powder and tooling. The stresses acting on the powder during the compaction process are also shown. Note that the pressures σ_T and σ_B have been defined in opposite direction to assure a non-zero compaction pressure.

mm/s, giving quasi-static conditions. The individual punches thus moved at a speed of 0.2 mm/s.

The following data results from a uniaxial compaction experiment: the total mass in the die m , the positions of the top punch z_T and bottom punch z_B , the force on the top punch F_T and bottom punch F_B , and the radial die-wall pressure σ_r . The mean pressures on the top and bottom face of the powder, σ_T and σ_B , are then calculated by dividing the force by the face area A of the punches. The compaction or axial pressure is then defined as

$$\sigma_z = \frac{\sigma_T + \sigma_B}{2}. \quad (3.1)$$

Furthermore, the distance between the two punches is denoted as H . A correction was applied to the punch positions because the punches slightly deform under pressure. Punches were also positioned such that the die-wall pressure sensor is always in the middle. The compaction density of the powder (including both elastic and plastic components) is then given by

$$\rho_m = \frac{m}{HA} = \frac{m}{V} \quad (3.2)$$

where V is the in-die volume of the powder.

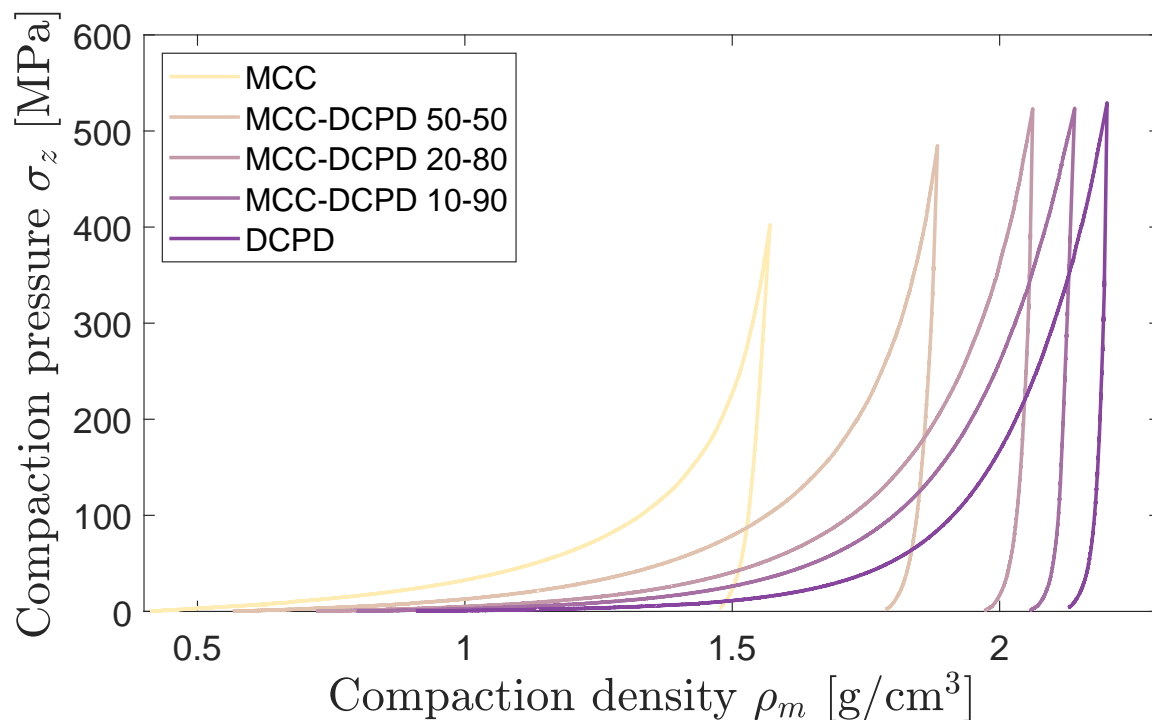


Fig. 3.3 An example compaction curve is shown for each material considered. At equal compaction pressures, the compaction density increases as the content of DCPD increases.

3.3 Automated preprocessing

To process the results of the compaction experiment, it is necessary to define a starting and ending point for each compaction curve. The chosen starting points also determine the value of ρ_0 in Eq. 3.15 and influence the calculated strain. An automated filtering method was thus implemented to improve reproducibility and user-convenience. The pressure data always starts with noise as the punches are not yet in contact with the powder. The standard deviation ξ in pressure of the first 120 ms is calculated. The start of the compaction curve is marked as the point where all points in the next 20 ms have a pressure above 6ξ . The end of the compaction curve is marked by the first point that is 1) past the peak compaction pressure, 2) below 10 MPa, and 3) has the standard deviation of the next 20 ms below 1.5ξ . This preprocessing was applied to all compaction data. Fig. 3.3 and 4.3 show that the preprocessing correctly selects compaction curves with minimal rejection of useful data.

There is a motivation for the difference in start and end criteria. The 6ξ threshold does not work at the end because compaction curves sometimes end with a constant pressure of a few MPa. Similarly, using the end criteria to define the start of the data would not work

because a random series of noisy data already has a high chance to have a standard deviation above 1.5ξ .

Precompaction is common in industrial settings but was not applied in the current study. The scripts were therefore already adapted to accommodate for data where precompaction has been applied. Precompaction means that the powder is slightly compacted and the punch retreats again before the main compression cycle. The precompaction step interferes with the parametrisation and is removed by only using data where the distance between the punches is smaller than the minimum observed during precompaction.

3.4 Extension of compaction curves

Closely inspecting experimental compaction curves shows that the maximum compaction density does not occur at the maximum compaction stress.[31, 35] The offset in compaction density is small, about 0.004 g/cm^3 , but is problematic because decompression therefore includes other behaviour than elastic recovery. Consequently, the compaction density is no longer monotonically decreasing during decompression. The parametrisation, which uses the slope of the decompression path, can thus result in near-infinite elastic moduli for some line segments. To avoid this problem the experimental compaction curves are extended before the parametrisation is applied (Fig. 3.4). This is done by fitting two linear splines through the compression and decompression part of the compaction curve, respectively. For decompression, the spline only uses data below 75% of the maximum compaction stress. A new maximum compaction stress is then computed as the intersection of the two splines. The procedure is iteratively repeated until the maximum compaction stress remains constant. The resulting extension then replaces the part of the compaction curve that lies between the original maximum compaction stress and the unloading point at 75% of the new maximum.

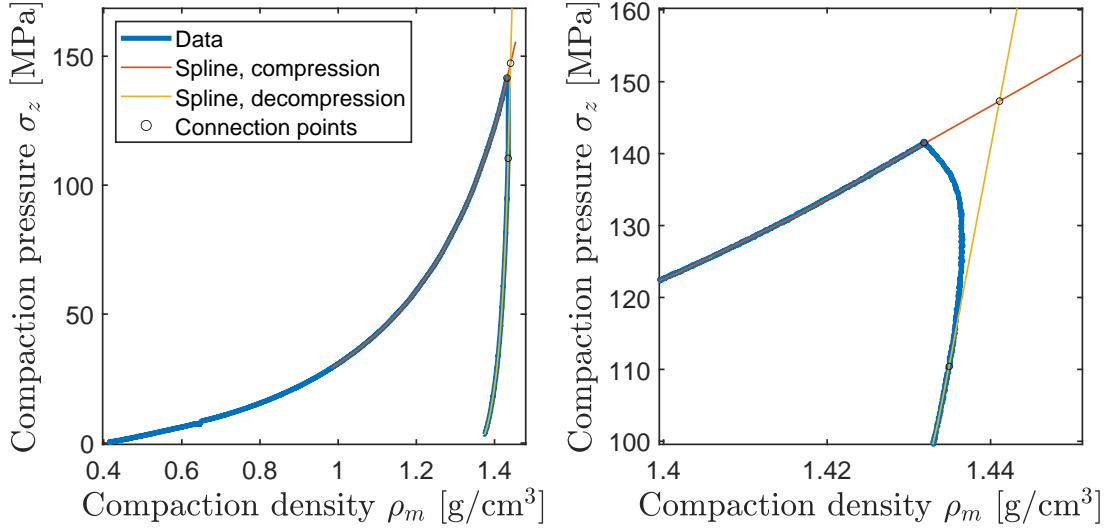


Fig. 3.4 An example of the compaction-curve extension procedure. The procedure enforces monotonicity of the decompression part of the compaction curve, which in turn ensures that the Young's modulus is always well-defined.

3.5 Quantitative comparison of compaction curves

To compare two different compaction curves quantitatively, the L1 loss function is introduced

$$L1 = \left(\int_{\rho_{start}^{ref}}^{\rho_{end}^{ref}} |\sigma_z - \sigma_z^{ref}| |d\rho_m| \right) \times \left(\max(\sigma_z^{ref}) \times \int_{\rho_{start}^{ref}}^{\rho_{end}^{ref}} |d\rho_m| \right)^{-1} \quad (3.3)$$

where one of the two curves, denoted with superscript *ref*, is considered to be the reference curve. The L1 loss function gives the deviation of a compaction curve with respect to a reference curve as an average per line segment, normalised by the peak compaction pressure. Eq. 3.3 gives a fraction but the L1 loss function is also frequently reported as a percentage. Using the L1 loss function, Fig. 3.5 shows that the variability between compaction curves is about 1 to 2% of the peak compaction pressure. The variability is higher for pure MCC because the gravity feeder was used instead of the force feeder. The gravity feeder produces larger deviations in the in-die mass. The L1 loss function is later used to quantify the deviation of simulations with respect to experiments.

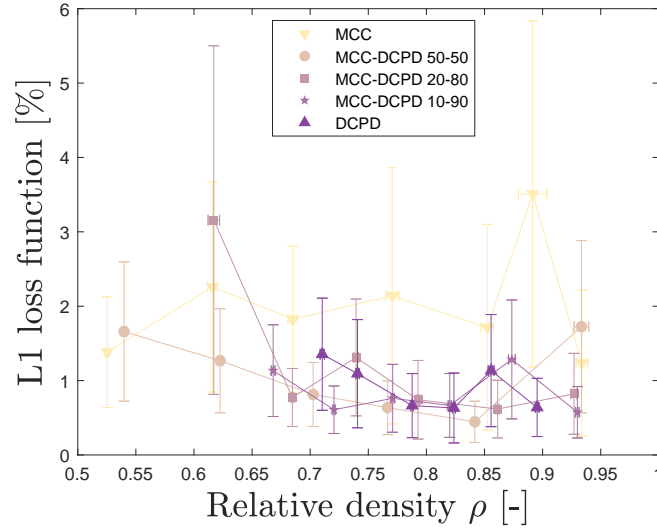


Fig. 3.5 The variability between experimental compaction curves hovers around 1 to 2% of the peak compaction pressure. Values are computed as the mean and standard deviation of all possible pairs of compaction curves with the same powder and target density.

3.6 Die wall friction

The friction between the powder and the die-wall significantly affects the stress distribution within the powder and has to be accounted for.[17, 19, 22, 23] Because the compaction experiments in this work use double-ended compaction (DEC) instead of single-ended compaction (SEC), a new expression for determining the friction coefficient μ is needed. Typical derivations make use of differential-slice or Janssen-Walker theory and start with the following force balance [17, 49]

$$\frac{\pi D^2}{4} d\sigma_z + \rho_m g \frac{\pi D^2}{4} dz = \tau_z \pi D dz. \quad (3.4)$$

Material	$\langle \mu \rangle$ [-]
MCC	0.1798
MCC-DCPD 50-50	0.1682
MCC-DCPD 20-80	0.1635
MCC-DCPD 10-90	0.1601
DCPD	0.1633

Table 3.1 Mean friction coefficients per material.

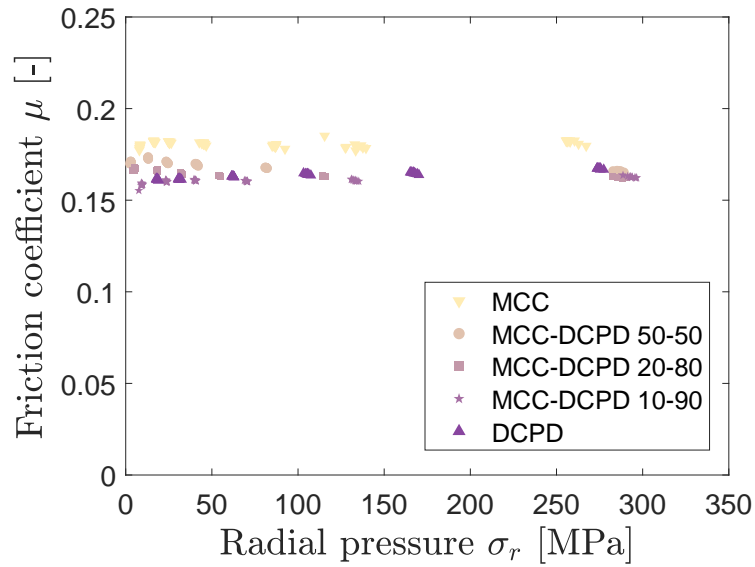


Fig. 3.6 The friction as a function of the radial pressure on the die-wall as given by Eq. 3.11.

The mass is negligible for pharmaceutical tablets and the second term is thus ignored. The materials is also assumed to be cohesionless. Next, it is assumed that the vertical stresses are uniformly distributed in a cylindrical cross-section with constant z and that the vertical and horizontal stresses are principal stresses. This gives

$$\sigma_r = \sigma_z K \quad (3.5)$$

with K being Janssen's constant. During compression, the failure mode of the powder within the die is always passive (i.e. inwards collapse). For an ideal Coulomb material this defines Janssen's constant as

$$K = \frac{1 + \sin(\beta)}{1 - \sin(\beta)} \quad (3.6)$$

with β the internal angle of friction. The friction coefficient is introduced using Coulomb's law of friction

$$\tau_z = \mu \sigma_r. \quad (3.7)$$

Combining the above expressions results in

$$\frac{d\sigma_z}{\sigma_z} = \frac{4\mu K}{D} dz. \quad (3.8)$$

Eq. 3.8 can be integrated to give the axial stress as function of the top-punch pressure σ_T and the distance z with respect to the top punch.

$$\sigma_z(z) = \sigma_T \exp\left(-\frac{4\mu Kz}{D}\right) \quad (3.9)$$

Reusing Eq. 3.5 gives

$$\frac{\sigma_r(z)}{K} = \sigma_T \exp\left(-\frac{4\mu Kz}{D}\right). \quad (3.10)$$

The final expression for the friction coefficient is then

$$\mu = \frac{D}{4zK} \ln\left(\frac{\sigma_T K}{\sigma_r}\right) \quad (3.11)$$

where z is the distance between the upper punch and the radial die-wall sensor. For DEC, the stress axial stress is symmetrical about the average of the two punch positions, where also the stress minimum is located. If the sensor is positioned below the average of the two punch positions then σ_T and z are substituted by the lower punch stress and distance, respectively.

3.7 True densities

Powders properties are often expressed as a function of the relative density ρ , which is the density of the powder relative to the same material with a porosity of zero. Therefore, the density of the non-porous material, called the true density ρ_t , has to be determined. The true density is determined using the method described by Sun.[50] A tablet is produced by compacting a powder up to a given target force. The minimum distance between the punches and maximum force are then recorded. This procedure is repeated for multiple target forces, three times per force. The data is collected by a script and the maximum compaction pressures and densities are calculated. The true density can then be determined using the

Material	ρ_t [g/cm ³]	R_{adj}^2
MCC	1.6374	0.994
MCC-DCPD 50-50	1.9661	0.995
MCC-DCPD 20-80	2.1882	0.995
MCC-DCPD 10-90	2.2635	0.997
DCPD	2.4380	0.995

Table 3.2 Results of fitting the Kuentz-Leuenberger model. The resulting true density and goodness of fit, reported as the adjusted R-squared, are given.

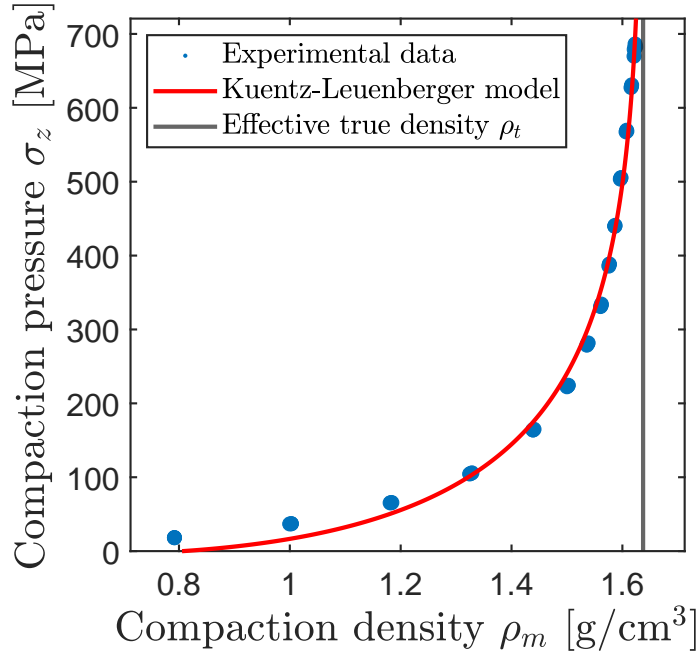


Fig. 3.7 An example of data and the fit used to determine the true density. MCC is shown here.

Kuentz-Leuenger model (also known as the modified Heckel model)[51]

$$\sigma = \frac{1}{C} \left(\frac{\rho_c - \rho_m}{\rho_t} - (1 - \rho_c) \ln \left(\frac{1 - \frac{\rho_m}{\rho_t}}{1 - \frac{\rho_c}{\rho_t}} \right) \right) \quad (3.12)$$

where ρ_m is the compaction density of the material, C a constant indicating the plasticity of the material, ρ_c the critical density at which the material starts to gain some strength or rigidity, and ρ_t is the true density of the material. The three fitting parameters, including the true density of the material, result from the fitting of Eq. 3.12 to the data.

3.8 Tensile strengths from crushing experiments

The tensile strengths of the produced tablets are also used to parametrise the model. The radial (or diametrical) tensile strength is given by

$$\sigma_r^f(\rho) = \frac{2F_{r,\max}}{\pi Dt} \quad (3.13)$$

and the axial tensile strength by

$$\sigma_z^f(\rho) = \frac{4F_{z,\max}}{\pi D^2} \quad (3.14)$$

where $F_{r,\max}$ is the maximum radial compression force, $F_{z,\max}$ the maximum axial compression force, D the tablet diameter, and t the tablet thickness. The Texture Analyser TA.XT.plusC (Stable Micro Systems, Surrey, United Kingdom) equipped with a 50 kg load cell was used to crush most tablets. However, the strength of some tablets exceeded the maximum force of the Texture Analyser and the Romaco Kilian STYL'One Evolution (Medelpharm, Beynost, France) was used instead. The radial and axial tensile were each determined for three tablets per density per material.

The tensile strength depends strongly on the relative density of the tablet. A common choice for describing this dependency is the Rhyshkewitch-Duckworth equation[46, 47, 52]

$$\sigma^f(\rho) = \bar{\sigma} \exp(-k_b(1 - \rho)) \quad (3.15)$$

where $\bar{\sigma}$ is the tensile strength at $\rho = 1$ and k is a constant representing the bonding capacity. The relative density ρ follows from the density of the tablet measured just before the tensile strength experiment. The value of ρ_0 is taken to be the lowest value of ρ of all compaction curves of that mixture. The resulting tensile strengths and fits of Eq. 3.15 can be seen in Fig. 3.8.

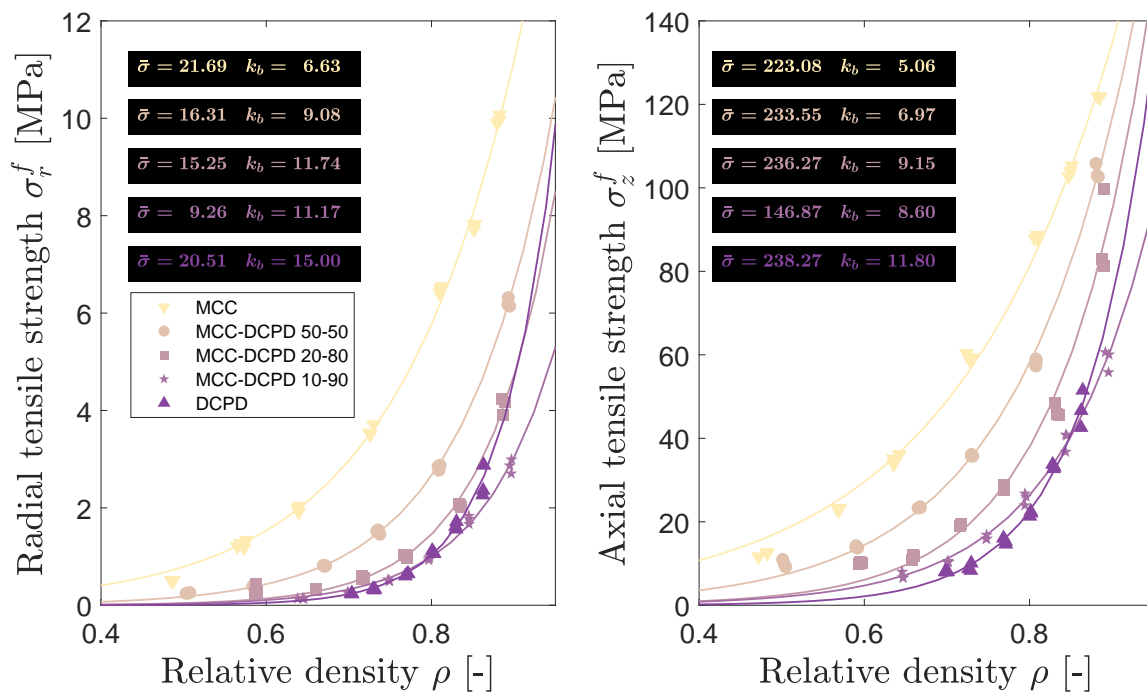


Fig. 3.8 The radial and axial tensile strengths as function of the relative density for each powder mixture. The curves and constants follow from a fit to Eq. 3.15.

Chapter 4

Defining material properties (direct parametrisation)

This chapter starts by describing the density-dependent Drucker-Prager Cap (dDPC) model that is used to define the powder behaviour in FEM simulations. Once the essential experimental data have been acquired, the next step is to extract the relevant dDPC model parameters from the data. In the simplest case, the parametrisation is a procedure that directly defines the dDPC model parameters of a material using the experimental data of that very same material. This will also be referred to as the direct parametrisation and is described in the current chapter. Particular care is taken to avoid *ad hoc* solutions, such that the described procedure can be automated and is valid for all materials considered. The proposed procedure is different from those proposed by previous authors but most closely resembles that of Garner et al.[34]

4.1 Density-dependent Drucker-Prager Cap (dDPC) model

First, the stress state of the material is described by the hydrostatic stress p ,

$$p = \frac{1}{3}(\sigma_1 + \sigma_2 + \sigma_3) = \frac{1}{3}(\sigma_z + 2\sigma_r), \quad (4.1)$$

and the von Mises equivalent stress q ,

$$q = \sqrt{\frac{(\sigma_1 - \sigma_2)^2 + (\sigma_2 - \sigma_3)^2 + (\sigma_3 - \sigma_1)^2}{2}} = |\sigma_z - \sigma_r|, \quad (4.2)$$

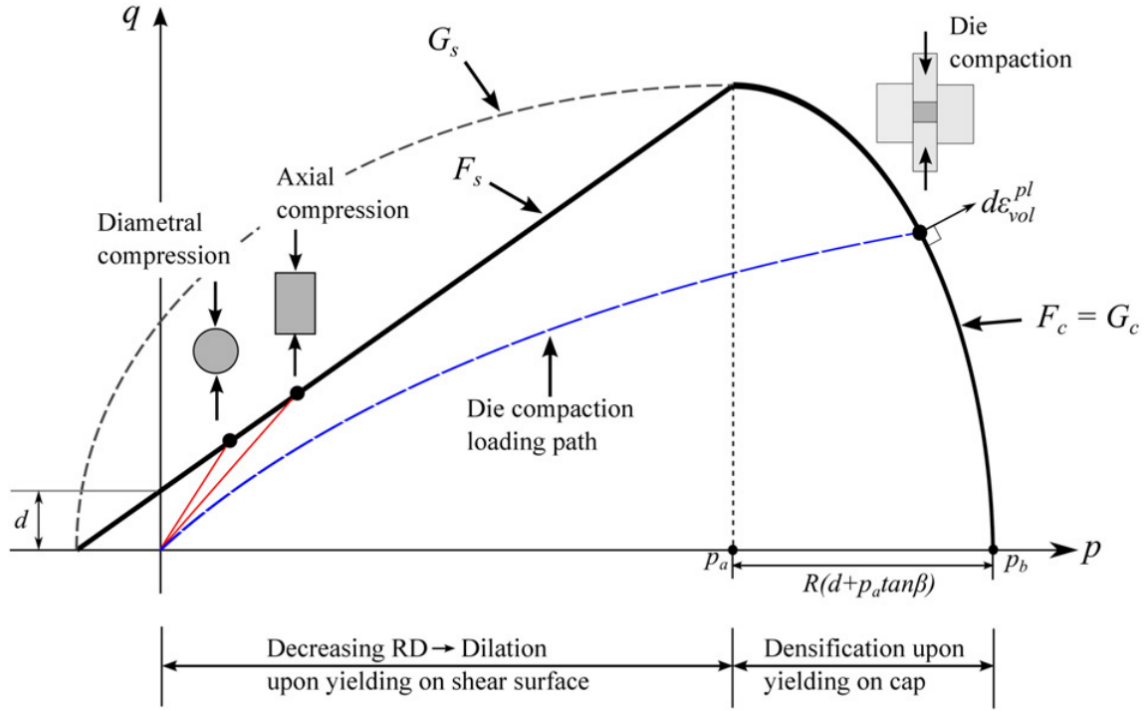


Fig. 4.1 A yield surface that is defined as a function of the hydrostatic (p) and Mises (q) stress as given by the Drucker-Prager Cap (DPC) model. The entire yield surface shifts depending on the density if the density-dependent DPC model is used. As illustrated, experiments can be used to obtain specific points on the yield surface. Figure taken from Garner et al.[34]

which have immediately been simplified for the case of axisymmetric and uniaxial compaction. The DPC model then defines a yield surface that consists of a shear failure segment F_s , a cap F_c , and a transition region F_t (Fig. 4.1).

Mohr-Coulomb theory is used to define the shear failure segment. The theory states that shear flow occurs if

$$F_s(p, q) = q - p \tan(\beta) - d = 0 \quad (4.3)$$

where, d is the cohesion, β the internal angle of friction, and compression is considered to give positive strain.

Aside from the shear failure mode, compressive flow or consolidation can occur. This happens on the cap of the model, which is given by a curve with constant eccentricity

$$F_c(p, q) = \sqrt{(p - p_a)^2 + \left(\frac{Rq}{1 + \alpha - \alpha/\cos\beta} \right)^2} - R(d + p_a \tan \beta) = 0 \quad (4.4)$$

where

$$p_a = \frac{p_b - Rd}{1 + R \tan \beta} \quad (4.5)$$

with p_b the hydrostatic yield stress on compression, R the cap eccentricity, and α a smoothing constant. The function p_b is generally considered to depend on the true volumetric plastic strain $\varepsilon_v^{\text{pl}}$

$$p_b = f(\varepsilon_v^{\text{pl}}) \quad (4.6)$$

and also called the cap-hardening curve. To aid numerical implementation, the shear failure segment and the cap are finally joined together by a smooth transition region

$$F_t(p, q) = \sqrt{(p - p_a)^2 + \left[q - \left(1 - \frac{\alpha}{\cos \beta} \right) (d + p_a \tan \beta) \right]^2} - \alpha (d + p_a \tan \beta) = 0. \quad (4.7)$$

The material thus undergoes plastic deformation if the stress state of the material is on or outside this yield surface. Otherwise, the material behaves purely elastically according to its Young's modulus E and Poisson's ratio ν .

The location of the DPC yield surface depends on the relative density ρ of the powder being compacted when using the dDPC model.[17, 20, 18] The DPC parameters d , β , R , and p_b are therefore made to be functions of the relative density, which is defined as

$$\rho = \rho_0 \exp(\varepsilon_v^{\text{pl}}) \quad (4.8)$$

with ρ_0 the relative density of the uncompacted powder in the die, before compression. The elastic properties E and ν are also taken to be density-dependent. It should be emphasized that the relative density is thus only dependent on the plastic deformation and not the elastic deformation.

The elastic and DPC material parameters for a given material can be obtained using the above information and the known experimental parameters σ_r^f , σ_r^f , σ_z , σ_r , m , A , and H that are described in chapter 3. The rest of this chapter describes how to obtain the dDPC parameters from experiment.

4.2 Cohesion and internal friction angle

The material cohesion d and internal friction angle β can be obtained from tensile strength experiments.[17] In tensile-strength experiments the tablets undergo shear-failure corresponding to diametrical and axial compression points on the shear line in Fig 4.1. The red lines through the origin and the diametrical and axial compression points have slopes of $3\sqrt{13}/2$

and 3, respectively. This gives $p = \frac{2}{3}\sigma_r^f$ and $q = \sqrt{13}\sigma_r^f$ for the radial strength and $p = -\frac{1}{3}\sigma_z^f$ and $q = -\sigma_z^f$ for the axial strength. It follows from Eq. 4.3 that

$$d = \frac{\sigma_z^f \sigma_r^f (\sqrt{13} - 2)}{\sigma_z^f - 2\sigma_r^f} \quad (4.9)$$

and

$$\beta = \tan^{-1} \left(\frac{3(\sigma_z^f + d)}{\sigma_z^f} \right). \quad (4.10)$$

Closed-form expressions for $d(\rho)$ and $\beta(\rho)$ are then obtained by substituting the tensile strengths σ_r^f and σ_z^f that follow from from Eq. 3.15 into Eq. 4.9 and 4.10.

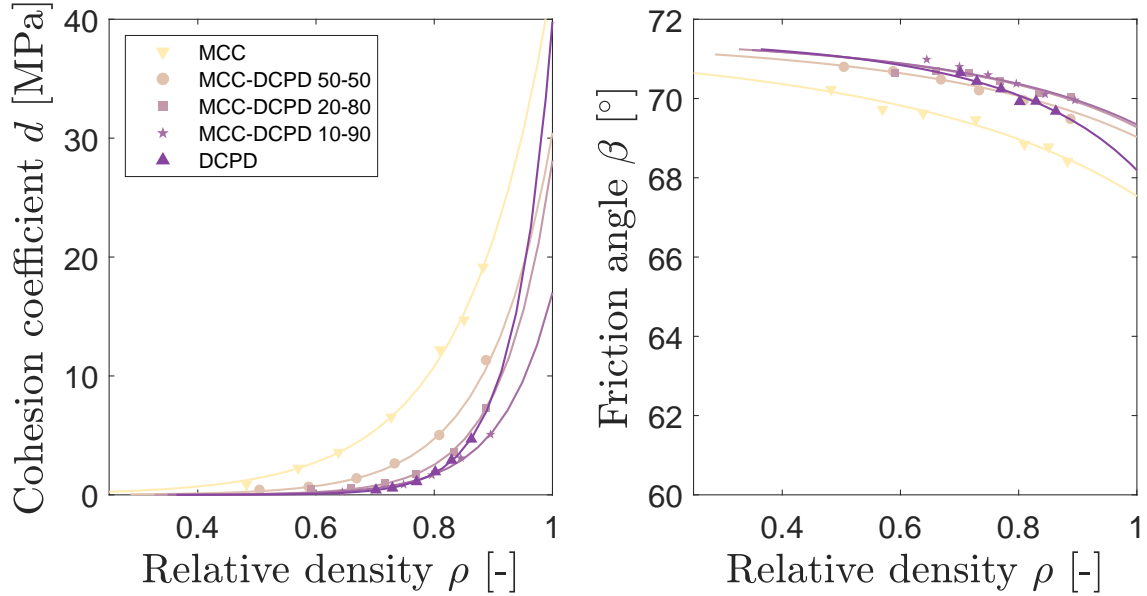


Fig. 4.2 The cohesion and friction angle as a function of the relative density for each powder mixture. Curves shown are the result of substituting the tensile strength relations (see Eq. 3.15 and Fig. 3.8) into Eq. 4.9 and 4.10.

4.3 Elastic parameters

The elastic parameters are determined using the segments AB in Fig. 4.3. It is widely presumed that the recovery of the tablet is purely elastic for this part of unloading.[12, 15, 20, 23] In this part of the curve both the hydrostatic and Mises stress are monotonically decreasing, making it less likely that internal tablet failure occurs. The slope of the σ_z - ε_z curve can then

be used to get an expression for E . The change in σ_z can be expressed as

$$d\sigma_z = M d\varepsilon_z = \left(K + \frac{4}{3}G \right) d\varepsilon_z = \frac{E(1-\nu)}{(1+\nu)(1-2\nu)} d\varepsilon_z \quad (4.11)$$

where M is the constrained modulus and the definitions of the bulk modulus

$$K = \frac{E}{3(1-2\nu)} \quad (4.12)$$

and the shear modulus

$$G = \frac{E}{2(1+\nu)} \quad (4.13)$$

have been substituted. Rearranging then gives

$$E = \frac{(1+\nu)(1-2\nu)}{(1-\nu)} \left(\frac{d\sigma_z}{d\varepsilon_z} \right). \quad (4.14)$$

Similarly, the slope of the AB segment of the σ_z - σ_r curve can be used to obtain to get an expression for ν . The change in σ_z can also be expressed as

$$d\sigma_z = \frac{3K+4G}{3K-2G} d\sigma_r = \frac{1-\nu}{\nu} d\sigma_r \quad (4.15)$$

which after rearranging gives

$$\nu = \frac{\left(\frac{d\sigma_r}{d\sigma_z} \right)}{1 + \left(\frac{d\sigma_r}{d\sigma_z} \right)}. \quad (4.16)$$

The Poisson's ratio ν is first obtained using Eq. 4.16 after which Eq. 4.14 is used to get the Young's modulus E . The currently available experimental data does not allow for extraction of reasonable nonlinear elastic parameters (i.e. E and ν as functions of the stress). For future studies, the procedure described by Mazel et al. is recommended for obtaining nonlinear elastic parameters.[32] Finally, it is emphasised that the elastic parameters are determined using true strains, as is conventional for systems experiencing large deformations.

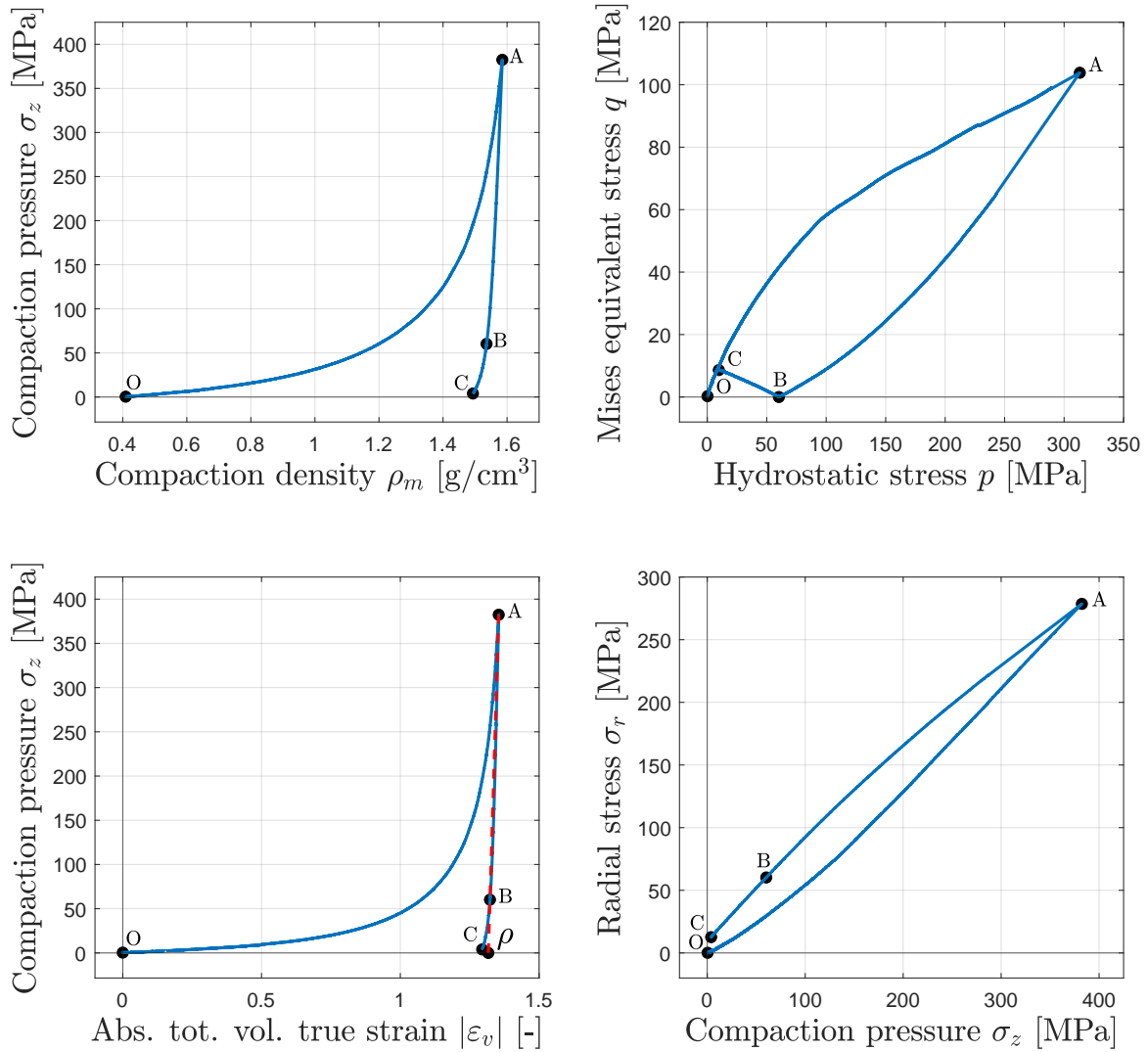


Fig. 4.3 This figure shows different data resulting from a single compaction experiment. Upper left: compaction curve used for validation. Upper right: p - q curve used to determine the DPC parameters R and p_b . Lower left: stress-strain curve used to determine the Young's modulus and relative density. Lower right: radial to axial stress plot used to determine the Poisson's ratio.

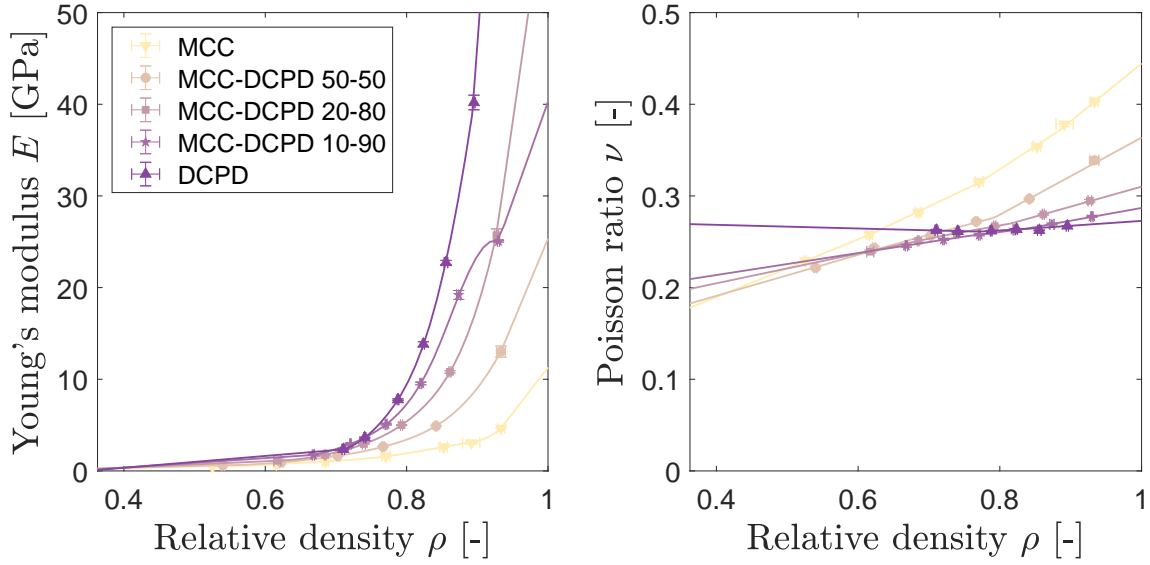


Fig. 4.4 The Young's modulus and Poisson's ratio as function of the relative density for each powder mixture. Symbols with error bars indicate the mean and standard deviation of the data. The curves are splines and extrapolations as described in section 4.6.

4.4 Relative density

The relative density is the main variable influencing material properties and should be determined with care. During ejection and the last stages of decompression (segment BC), the tablet may undergo shear failure.[19] The Mises stress increases along segment BC and can thus reach the shear failure line in some cases. This can change the relative density of the tablet or make the measurement thereof infeasible because the tablet fails. Therefore, the true density is estimated by subtracting the elastic true volumetric strain from the maximum compression point A . Only the true volumetric plastic strain remains, which is directly related to the true density, and will likely not have been affected by tablet failure during decompression.

Recall that compression is considered to give positive strain and elasticity is assumed to be linear. Using Eq. 4.11, the elastic strain at point A is given by

$$\varepsilon_v^{\text{el}} = \varepsilon_z^{\text{el}} = \int_0^{\sigma_{z,A}} \frac{1}{M} d\sigma_z = \frac{\sigma_{z,A}}{M} \quad (4.17)$$

and the total strain is given by

$$\varepsilon_v^{\text{tot}} = \varepsilon_z^{\text{tot}} = \ln\left(\frac{H}{H_0}\right) = \ln\left(\frac{\rho_{m,A}}{\rho_0\rho_t}\right). \quad (4.18)$$

Eq. 4.17 and 4.18 can then be combined with Eq. 4.8 to give

$$\rho = \rho_0 \exp(\varepsilon_v^{\text{pl}}) = \rho_0 \exp(\varepsilon_v^{\text{tot}} - \varepsilon_v^{\text{el}}) = \frac{\rho_{m,A}}{\rho_t} \exp\left(-\frac{\sigma_{z,A}}{M}\right). \quad (4.19)$$

The red dashed line in Fig. 4.3 illustrates how the relative density ρ is determined starting from point A.

4.5 Plastic parameters

The plastic parameters R , p_a , and p_b are considered next. Point A in Fig. 4.3, the stress peak, is generally considered to be located on the yield surface. Eq. 4.4 therefore applies at point A, which means that $F_c(p_A, q_A) = 0$. Associated with Eq. 4.4 is also a plastic flow potential component:

$$G_c = \sqrt{(p - p_a)^2 + \left(\frac{Rq}{1 + \alpha - \alpha/\cos\beta}\right)^2} \quad (4.20)$$

The associative flow rule in the radial direction is

$$d\varepsilon_r^{\text{pl}} = d\lambda \left. \frac{\partial G_c}{\partial \sigma_r} \right|_{p_A, q_A} \quad (4.21)$$

with $d\varepsilon_r^{\text{pl}}$ the change in radial plastic strain, $d\lambda > 0$ the magnitude of the plastic deformation, and the derivative of G_c indicating the direction. Furthermore, the die wall is assumed to be a non-deformable rigid body giving $d\varepsilon_r^{\text{pl}} = 0$. It follows that the change in G_c at this point is also zero:

$$\left. \frac{\partial G_c}{\partial \sigma_r} \right|_{p_A, q_A} = 0. \quad (4.22)$$

Eq. 4.22 can then be combined with Eqs. 4.1, 4.2, and 4.20 to give

$$R = \sqrt{\frac{2(1 + \alpha - \alpha/\cos\beta)^2}{3q_A}} (p_A - p_a). \quad (4.23)$$

Hereafter, Eq. 4.23 is substituted back into Eq. 4.4 to also obtain

$$p_a = -\frac{3q_A + 4d(1 + \alpha - \alpha/\cos\beta)^2 \tan\beta}{4[(1 + \alpha - \alpha/\cos\beta) \tan\beta]^2} + \frac{\sqrt{9q_A^2 + 24q_A d(1 + \alpha - \alpha/\cos\beta)^2 \tan\beta + 8(3p_A q_A + 2q_A^2)[(1 + \alpha - \alpha/\cos\beta) \tan\beta]^2}}{4[(1 + \alpha - \alpha/\cos\beta) \tan\beta]^2}.$$

Rearranging Eq. 4.5 finally gives an expression for the hydrostatic yield stress

$$p_b = p_a(1 + R \tan\beta) + Rd, \quad (4.24)$$

where the value of α is relatively unimportant and set to a constant 0.03 in accordance with previous authors.[15]

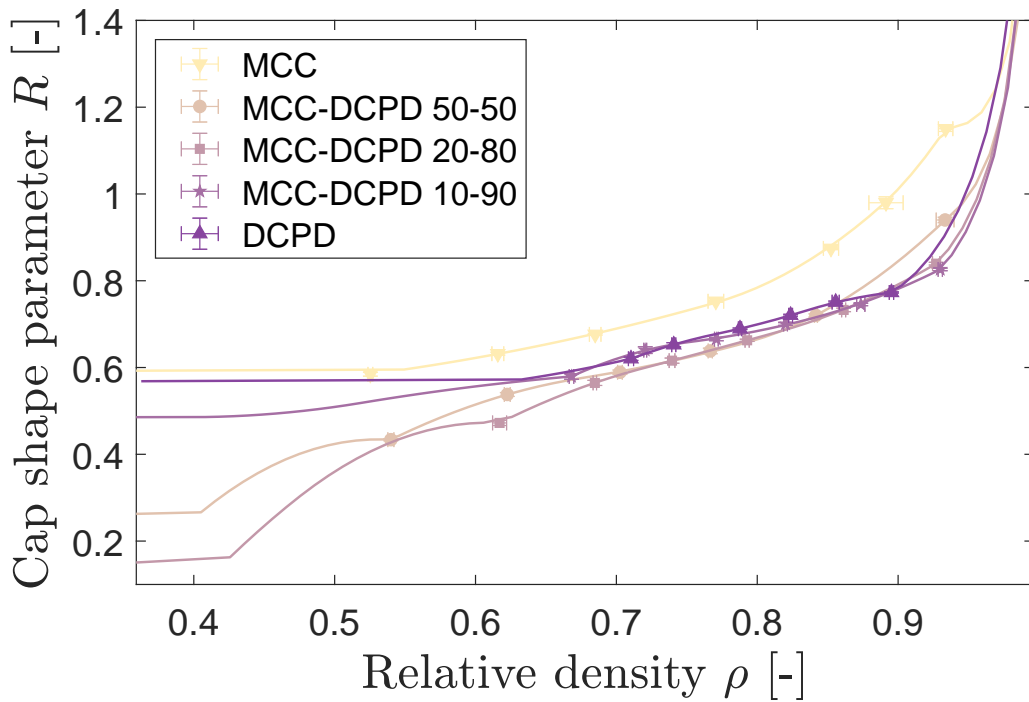


Fig. 4.5 The cap-shape parameter R as function of the relative density for each powder mixture. Symbols with error bars indicate the mean and standard deviation of the data. The curves are splines and extrapolations as described in section 4.6.

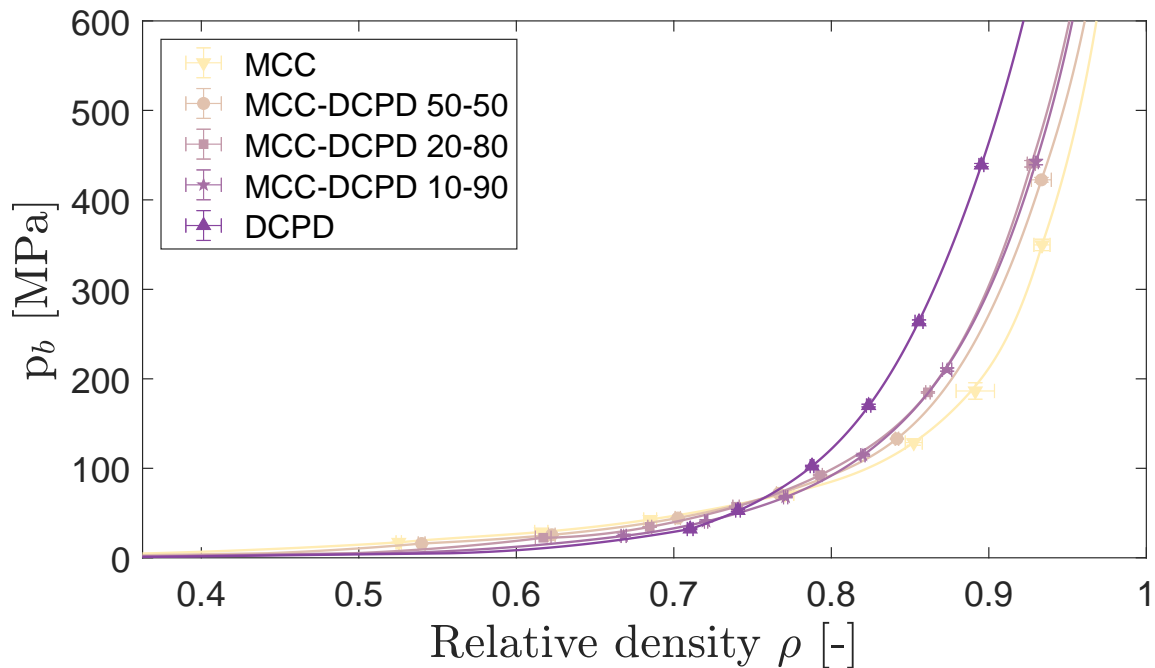


Fig. 4.6 The hydrostatic yield stress p_b as function of the relative density for each powder mixture. This function is also called the cap hardening curve. Symbols with error bars indicate the mean and standard deviation of the data. The curves are splines and extrapolations as described in section 4.6.

4.6 Fitting and extrapolating the DPC parameters

Because the FEM simulations should follow the experimental compaction curves as closely as possible, the parametrisation should follow the trend in experimental material parameters as closely as possible. This necessitates an appropriate fitting and interpolation method. It was found that analytical models were incapable of sufficiently describing the data for all materials. Therefore, to retain generality, all parameters were fit using quadratic B-splines with a number of breaks equal to half the number of target densities, rounded to the nearest integer.[53] There are two exceptions, linear splines were used for v and cubic splines for p_b . Splines were also forced to go through the mean values of the parameters at the minimum and maximum target density to enforce continuity with the extrapolations.

Physical extrapolations are also needed. First, because the simulations start at a density lower than the minimum observed tablet density. And second, because some areas of the tablet will reach densities higher than the mean density at maximum compaction. The extrapolation methods proposed by Garner et al. were used for the dDPC parameters.[34] In

short, low-density extrapolations are done by fitting the function

$$\rho(\rho_m, \rho_t, \rho_0) = a \left(\frac{\rho_m}{\rho_t} - \rho_0 \right) + b \left(\frac{\rho_m}{\rho_t} - \rho_0 \right)^2 \quad (4.25)$$

using the known relative densities at maximum compaction, where a and b are constants. This function is then used to compute estimations of the DPC parameters along the low-density end of the compaction curves. The estimated dDPC parameters are then fit using the same B-splines as previously mentioned. The high-density extrapolations are based on the modified Gurson model and the physical requirement that p_b and R should tend to infinity for a relative density of one. The low- and high-density extrapolations are forced to go through the lowest and highest target density, respectively, to enforce continuity.

The elastic parameters were extrapolated as follows. For the Young's modulus, the low-density extrapolation is given by a straight line through $E = 0.1$ GPa at ρ_0 and the mean Young's modulus at the lowest target density. Using a minimum value for E that is much lower than 0.1 GPa causes the powder not to compact during the FEM simulations. For the high-density extrapolations, a limiting value $E(\rho = 1)$ is determined. The data is fit to two models for porous materials, the Hashin-Hasselman model and the model by Nachtrab.[54, 55] The value of $E(\rho = 1)$ is then given by the model with the best fit. The high-density extrapolation is then given by a straight line from the mean Young's modulus at the highest target density to $E(\rho = 1)$. The extrapolations for the Poisson's ratio followed directly from the linear spline used to fit the data.

Aside from sufficiently physical extrapolations, a number of additional requirements were found to be essential to assure physical and numerically stable results at the same time. First, p_b needs a minimum value and a significant slope. This was done by setting $p_b(\rho_0) = 1.0$ MPa and then drawing a straight line to the first point for which $p_b > 5.0$ MPa. Second, p_b and R need to be monotonically increasing. Any decreasing values in p_b or R were therefore replaced by linear interpolations to the next larger value.

The parameter inter- and extrapolations can be seen alongside the data in Fig. 4.2, 4.4, 4.5, and 4.6. Parameters d and β were excluded from the aforementioned procedures because their functions had already been set through Eq. 3.15, 4.9, and 4.10.

Finally, although p_b has been defined as a function of ρ , the Abaqus software requires $p_b(\varepsilon_v^{\text{pl}})$ as cap-hardening curve. This can be solved by a transformation. The volumetric plastic strain is directly related to the relative density, as follows from Eq. 4.8:

$$\varepsilon_v^{\text{pl}}(\rho) = \ln \left(\frac{\rho}{\rho_0} \right), \quad (4.26)$$

where ρ_0 is the relative density of the uncompacted powder in the die, before compression. The function $p_b(\rho)$ is thus converted using Eq. 4.26, giving

$$p_b = f(\varepsilon_v^{\text{pl}}) = f\left(\ln\left(\frac{\rho}{\rho_0}\right)\right). \quad (4.27)$$

Chapter 5

Estimation of mixture properties (indirect parametrisation)

Having described a generalised procedure to obtain dDPC model parameters from experiment, the next improvement is the definition of a method that successfully predicts the dDPC parameters of a binary mixture. In particular, the method should only use experimental data of the single-component powders. This chapter will propose two such methods. The first is to create a (microscopically-)segregated composite that is sufficiently descriptive of the mixture. The second is to define a set of rules that mixes the dDPC model parameters of two single-components powders to get the parameters of a binary powder mixture. Both approaches are referred to as indirect parametrisation methods because the methods do not use any experimental data of the mixtures to predict their properties.

5.1 True density and volume fraction

Regardless of the chosen method, the volume fraction per component and the true density of the mixture are needed.

The true density of a mixture can be estimated using the volumetric mixing rule

$$\rho_{t,\text{mix}} = \left(\sum_i \frac{w_i}{\rho_{t,i}} \right)^{-1} \quad (5.1)$$

where $\rho_{t,i}$ and w_i are the true density and weight fraction of the respective constituent material.[50] The deviations of Eq. 5.1 with respect to the experimental true densities are +0.4, -1.5, and -2.7 % for the 50-50, 20-80, and 10-90 mixtures, respectively. Eq. 5.1 is therefore considered to be accurate, as was also demonstrated by Wu et al.[46]

The volume fraction of component i within the mixture can be estimated using[47]

$$y_i = \left(\frac{w_i}{\rho_i \rho_{t,i}} \right) \left(\sum_j \left(\frac{w_j}{\rho_j \rho_{t,j}} \right) \right)^{-1}. \quad (5.2)$$

5.2 Reynolds et al. model

Before introducing the new methods, the Reynolds et al. model is briefly described.[47] This is the simplest of the models that gives a prediction of the density of a mixtures as function of the compaction pressure. The model cannot predict decompression behaviour or give more detailed information such as the stress and density profiles within the tablet. This limits the ability of the model to help identify and prevent tablet defects in production, especially when there are strong restrictions on the composition of the powder. However, this model provides a good reference points for comparison with the new methods.

In short, the Reynolds model assumes the individual materials within the composite are ordered like a checker board. This results in isostress conditions. The densities of the individual components are then expressed as a function of the stress. The mixture density is then given as a volumetric average of the individual component densities. The Reynolds et al. prediction of the compaction curve of a mixture is thus given by

$$\frac{\rho_m(\sigma)}{\rho_t} = \sum_i \frac{y_i \rho_{m,i}(\sigma)}{\rho_{t,i}}, \quad (5.3)$$

which for a binary mixture becomes

$$\frac{\rho_m(\sigma)}{\rho_t} = \frac{y_1 \rho_{m,1}(\sigma)}{\rho_{t,1}} + \frac{y_2 \rho_{m,2}(\sigma)}{\rho_{t,2}} = \frac{y_1 \rho_{m,1}(\sigma)}{\rho_{t,1}} + \frac{(1 - y_1) \rho_{m,2}(\sigma)}{\rho_{t,2}} \quad (5.4)$$

where the identity $y_2 = 1 - y_1$ has been used. The full details can be found in the original paper.[47]

5.3 Layered or (microscopically-)segregated tablets

The first method proposed is to simulate a tablet with distinct regions of pure MCC and DCPD. However, the way that the stress distributes itself will strongly depend on the spatial arrangement of the regions of MCC and DCPD within the tablet. For example, fully horizontal or vertical layers will approximately correspond to a composite under isostress or isostrain conditions, respectively. Simulating a number of layered tablets with different

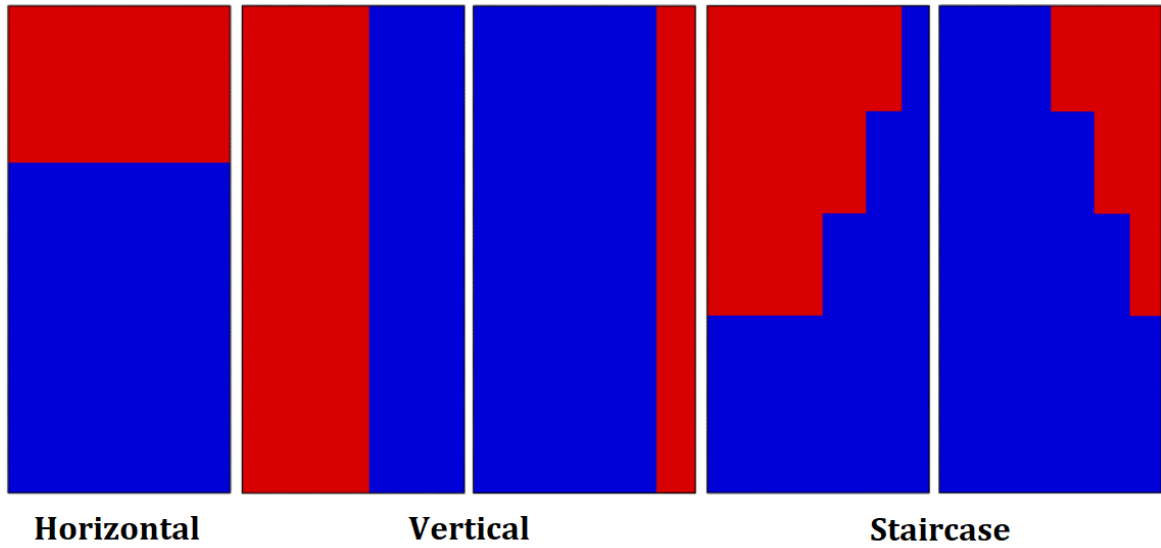


Fig. 5.1 Initial spatial arrangements for the layered tablets that have been considered in this study. All tablets are 50-50 MCC-DCPD. Blue indicates the MCC powder whereas red indicates the DCPD powder. Note that the volume of the layers differs because of the difference in density.

spatial arrangements is therefore necessary and will provide information about the mechanical interaction between the two materials. Fig. 5.1 shows the spatial arrangements considered, which are all bilayers. The simulation of layered tablets also requires a number of adjustments to the model that are discussed in the rest of this section.

For all mixtures it was observed that

$$\rho_{m,0,tot} \neq y_1\rho_{m,0,1} + y_2\rho_{m,0,2}, \quad (5.5)$$

which means that the starting density of the individual layers has to be adjusted to ensure mass conservation. To enforce conservation, the relative density of all components is changed by an equal amount,

$$\rho_i = \rho_{0,i} + \delta, \quad (5.6)$$

under the mass-conservation constraint

$$\rho_{m,0,tot} = y_{0,1}\rho_{m,0,1} + y_{0,2}\rho_{m,0,2} \quad (5.7)$$

where $\rho_{m,0,i}$ is the minimum density of the powders in g/cm^3 and $y_{0,i}$ is the estimated initial volume fraction. The value of $y_{0,i}$ follows from Eq. 5.2 with $\rho_i = \rho_{0,i}$ for all i . Substitution

of Eq. 5.6 into Eq. 5.7 and using $\rho_{m,0,i} = \rho_{0,i}\rho_{t,i}$ gives

$$\delta = \left(\rho_{m,0,tot} - \sum_i y_{0,i} \rho_{0,i} \rho_{t,i} \right) \left(\sum_i y_{0,i} \rho_{t,i} \right)^{-1}. \quad (5.8)$$

Eq. 5.6 and Eq. 5.8 now define the initial relative density of a layer. Furthermore, because the starting density of the individual materials is no longer $\rho_{0,i}$ this also means that the initial plastic strain $\varepsilon_{v,0,i}^{pl}$ has to be adjusted (since it is no longer zero). This property is called the initial yield surface position within Abaqus and can be computed using Eq. 4.8. Interaction between the layers is automatically defined as the layers are not allowed to overlap. The only exceptions are the friction and cohesion between the layers. Hancock et al. found that the friction coefficient μ between two tablets is typically of the order of 0.01.[56] The friction coefficient between the layers is therefore set to $\mu = 0.01$. Even for such low values of μ , the layers show minimal slippage before the end of the decompression stage. The cohesion between the different materials is less straightforward to determine and is neglected in the present study.

5.4 Mixing rules

The second method proposed makes use of mixing rules. Under the assumption that isostress conditions are most suitable, a set of mixing rules was developed to predict the elastic and dDPC parameters for an arbitrary mixture.

All model parameters depend on the relative density but now have to be expressed as a function of the stress to adhere to the isostress condition. Therefore, the compaction density of each single-component powder i is expressed as a function of stress by fitting a spline, $\rho_{m,i}(\sigma)$. The spline $\rho_{m,i}(\sigma)$ is then substituted into Eq. 4.25 to get $\rho_i(\sigma)$. The function $\rho_i(\sigma)$ is then substituted into the previously-determined parameter functions to define all material parameters of a component i as a function of the stress.

Since the volume fractions of each component are not constant during compression, these also have to be determined. The total strain per component is

$$\varepsilon_{v,i}(\sigma) = \varepsilon_v^{el} + \varepsilon_v^{pl} = \int_0^\sigma \frac{1}{M_i(\rho_i(\sigma))} d\sigma + \ln \left(\frac{\rho_i(\sigma)}{\rho_{0,i}} \right) \quad (5.9)$$

where Eq. 4.17 and 4.26 have been substituted. The constrained modulus M_i follows from the known functions for the elastic parameters and Eq. 4.11. These strains define the change in volume for each component and can thus be used to determine the volume fraction as a

function of stress as well.

$$y_i(\sigma) = y_{0,i} \exp(-\varepsilon_{v,i}(\sigma)) \left(\sum_j y_{0,j} \exp(-\varepsilon_{v,j}(\sigma)) \right)^{-1} \quad (5.10)$$

Finally, the density of the mixture follows as

$$\rho(\sigma) = \frac{1}{\rho_t} \sum_i y_i(\sigma) \rho_i(\sigma) \quad (5.11)$$

and the value of any property θ for the mixture is given by

$$\theta(\rho) = f(\theta_1(\rho_1), \dots, \theta_n(\rho_n), y_1(\rho_1), \dots, y_n(\rho_n)) \quad (5.12)$$

with $f(\dots)$ being the appropriate mixing rule.

In accordance with the isostress model, the mixing rules for the Young's modulus and the Poisson's ration are as a harmonic and an arithmetic mean, respectively. For all other parameters the arithmetic mean is used. The arithmetic mean is $f(\theta_1(\rho_1), \dots, \theta_n(\rho_n)) = \sum_i y_i(\rho_i) \theta_i(\rho_i)$. And the harmonic mean is $f(\theta_1(\rho_1), \dots, \theta_n(\rho_n)) = \left(\sum_i \frac{y_i(\rho_i)}{\theta_i(\rho_i)} \right)^{-1}$. The exact mixing rule applied on the plastic parameters appears to make little difference to the eventual results because, at the same stress, the yield loci for the different materials are already very close to each other.

Chapter 6

FEM and numerical modelling details

This chapter describes the FEM simulation set-up and numerical implementation of the dDPC model. The commercial software Abaqus 2019 by Simulia was used for all FEM simulations and subroutines were used to implement the dDPC model. Note that units within Abaqus are arbitrary but need to be consistent. The units used here are N, mm, MPa, degrees, and for the density kg/mm^3 .

6.1 Geometry and meshing

The FEM model was made to mimic the experimental compaction process as much as possible. The in-die and punch diameters were thus 11.28 mm. The crushing plates were 12.28 mm to avoid overhang of the tablet. The compaction profile was a V-shaped DEC profile. The initial height of the powder and the final compaction height were set to the averages of all compaction experiments with the same target density. Note that the final density of a tablet is mainly determined by the initial height of the powder, as the final compaction heights are approximately equal.

All parts of the model were represented as axisymmetric deformable bodies. Also making the tooling deformable bodies has two advantages; it improves the numerical stability and facilitates future extensions that aim to include heat transfer. A uniform, regular mesh with square elements was used for the powder, the punches, and the crushing plates. The mesh for the powder consisted of 4312 to 7840 elements, depending on the initial height of the powder. The punch meshes had 376 elements and the crushing plate meshes had 432 elements. The die was given an irregular mesh made out of rectangular as well as triangular elements (because of the curved edges) with a total of 1294 elements. The punches, die wall, and crushing plates were made to be 1 mm thick and given the properties of tooling steel ("Elastic": $E = 210 \text{ GPa}$, $\nu = 0.3$, "Plastic": yield stress going from 1400 to 1800 MPa for

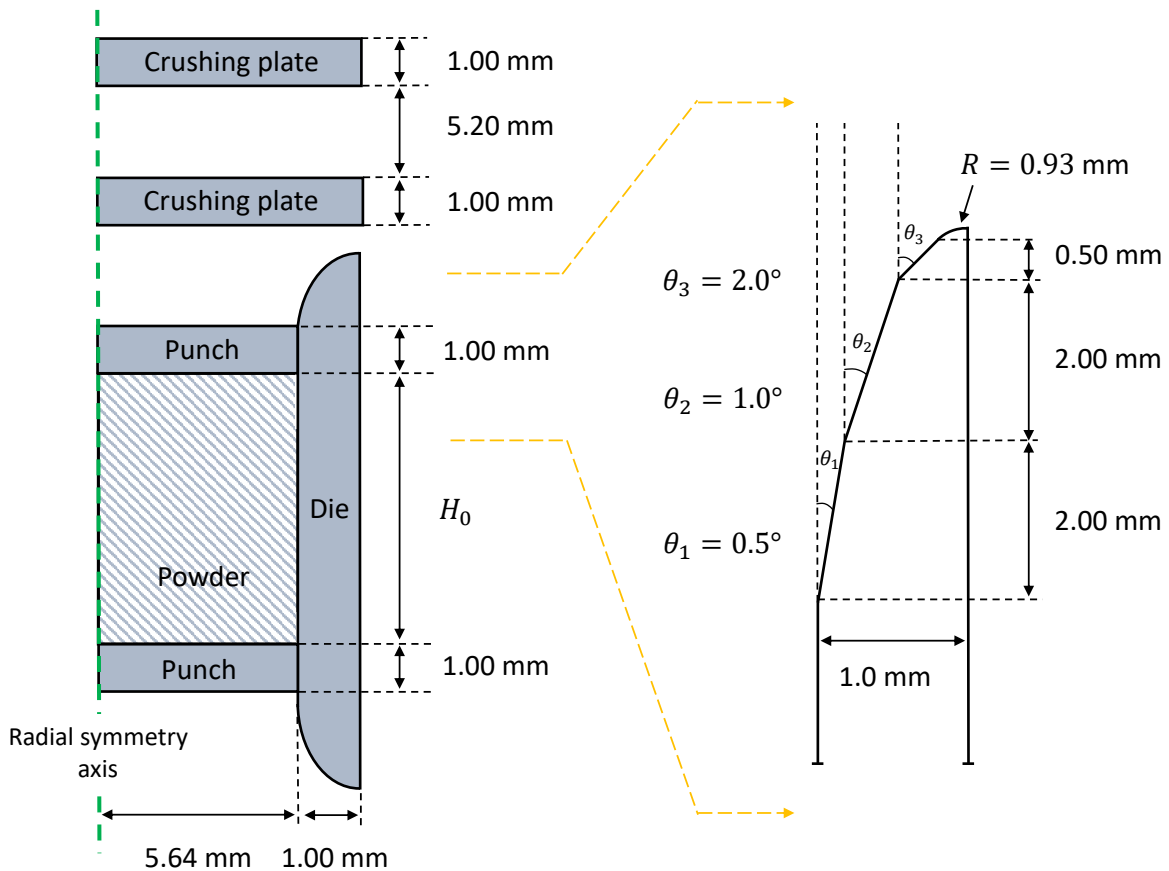


Fig. 6.1 Schematic drawing of the tooling geometry at the beginning of the simulation. The crushing plates do not interact with the powder until after ejection, when the tablet has been moved to a position in between the crushing plates. The gradient of the die wall is continuous at the point where the tapering starts to curve outwards. Dimensions are not to scale.

a plastic strain going from 0 to 0.4, and "Density": 7900 kg/m³).[57] Boundary conditions were applied to the outer surfaces of the punches and die. This means that the outer surface of the die was fixed and displacements were applied on the top of the top punch and bottom of the bottom punch.

In the case of materials with a very low cohesions and friction angles, the tablet can strongly bend upon ejection due to the sudden release of residual radial pressure. Such tablet bending does not allow for proper numerical crushing experiments. Tapering was therefore added to give a smoother release of the residual radial pressure and avoid excessive bending of the tablet. For some high-density tablets, the initial height of the powder can cause the powder to rise above the starting point of the tapering. However, compaction simulation

with and without tapering show that this has no visible effect on the resulting compaction pressures and density profiles.

Fig. 6.2 shows that the used combination of the parametrisation and model geometries gives excellent convergence.

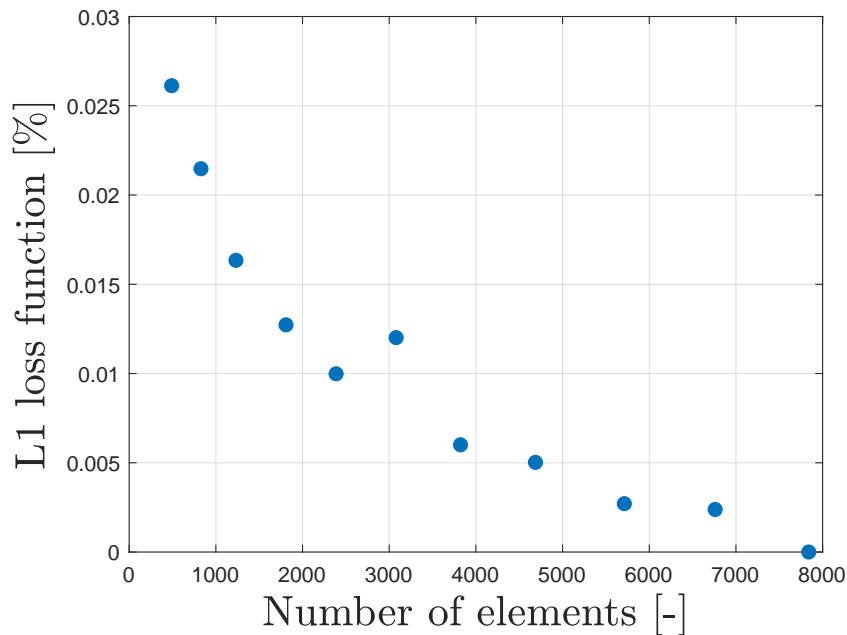


Fig. 6.2 Convergence of the resulting compaction curves with respect to the number of mesh elements. The simulation with the highest number of elements is used as the reference for computing the L1 loss function. All simulations featured compaction of MCC to the highest target density. The error in the compaction curves due to mesh resolution is negligible.

6.2 Numerical integration

Time step integration was performed using the dynamic implicit scheme with the quasi-static option. The amplitude of the boundary conditions was given as a smooth ramp over time per step (loading, unloading, ejection, crushing). Reduced element integration was disabled, giving the CAX3 or CAX4 element type for the chosen axisymmetric representation. The option NIgeom was on, making all strain definitions be true strains (and not engineering strains).

6.3 Powder properties and subroutine

Mechanical properties of the powder bed were set according to the parametrisation described in chapters 4 and 5. The required keywords are "Cap Plasticity", "Cap Hardening", "Density", "Depvar", "Elastic", and "User Defined Field". The MATLAB parametrisation script gives the tabulated material properties that can then be directly copy-pasted into Abaqus. The flow-stress ratio was set to 1 in correspondence with the dDPC model.

The keywords "Depvar" and "User Defined Field" enable the FORTAN subroutine USDFIELD that allows the definition of the relative density as a new field variable. This is necessary to make the DPC model parameters dependent on the relative density. For each individual node, the relative density is given by

$$\rho(t) = \rho_0 \exp\left(-\min\left(\varepsilon_v^{\text{pl}}(0), \dots, \varepsilon_v^{\text{pl}}(t)\right)\right) \quad (6.1)$$

where $\varepsilon_v^{\text{pl}}$ is given by variable PEQC(4). Eq. 6.1 follows from Eq. 4.8 except that the sign of the plastic strain changes because Abaqus internally defines strain to be negative for compression. Furthermore, the constraint that ρ is only allowed to increase was added to assure stability of the simulation. Without this constraint, the relative density is monotonically increasing during compression and decreases negligible amounts during decompression. However, in the case of low-cohesion materials, the tablet can strongly shear upon ejection. This causes the relative density to decrease, which in turn lowers the cohesion, causing a positive feedback loop that leads to numerical instability and excessive dilation of the tablet. The aforementioned constraint was therefore added. The effect of shear yielding upon ejection can still be observed through the plastic deformation.

Friction and normal interactions are added between the surfaces of the powder and tooling that come into contact with each other. A penalty friction type is used with a constant friction coefficient. Normal behaviour is given as an exponential pressure-overclosure with pressure 10 and clearance 0.002. In the case of a layered tablet, the interaction between the two powder meshes is defined in the same way.

6.4 Output

The compaction pressure is given by the mean force on the punches divided by the punch area (see section 3.2). Similarly, the compaction density is given by

$$\rho_m = \frac{m}{V} = \frac{m}{HA} \quad (6.2)$$

where V is the in-die volume and A is the face area of the tablet.

During the crushing of the tablet, the stress on each plate is computed by dividing the force on the plate by the contact area between the plate and the tablet. The yield stress is then compute from the average stress on the top and bottom plate at yield. The tablet is considered to yield when there is a path of fully-yielding elements (as indicated by the variable AC YIELD) either vertically or horizontally across the tablet.[28] In some cases this may occur at very low stresses, because the tablet has slightly bent during ejection. This can be recognised by pure shear yield (AC YIELD 1) with an irregular yielding pattern and is ignored when determining the yield stress.

Element averaging of the output was disabled when visualising field variables (e.g. the stress profile of the tablet).

Chapter 7

Results and discussion

7.1 Direct parametrisation

7.1.1 Validation of the direct method

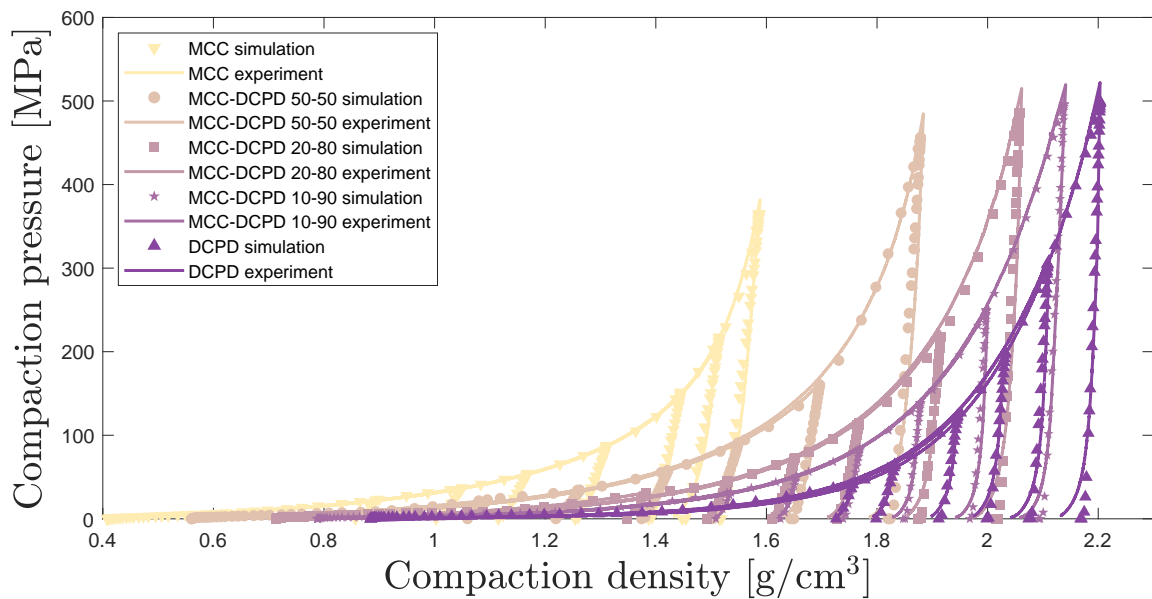


Fig. 7.1 FEM simulations using direct parametrisation follow the experimental data closely for all materials and target densities. One experimental curve is shown per unique combination of material and target density. Symbols indicate the compaction curve as predicted by FEM simulations.

To validate the automated parametrisation method proposed in chapter 4, FEM simulations of the compaction process of each material were done using the set-up as described

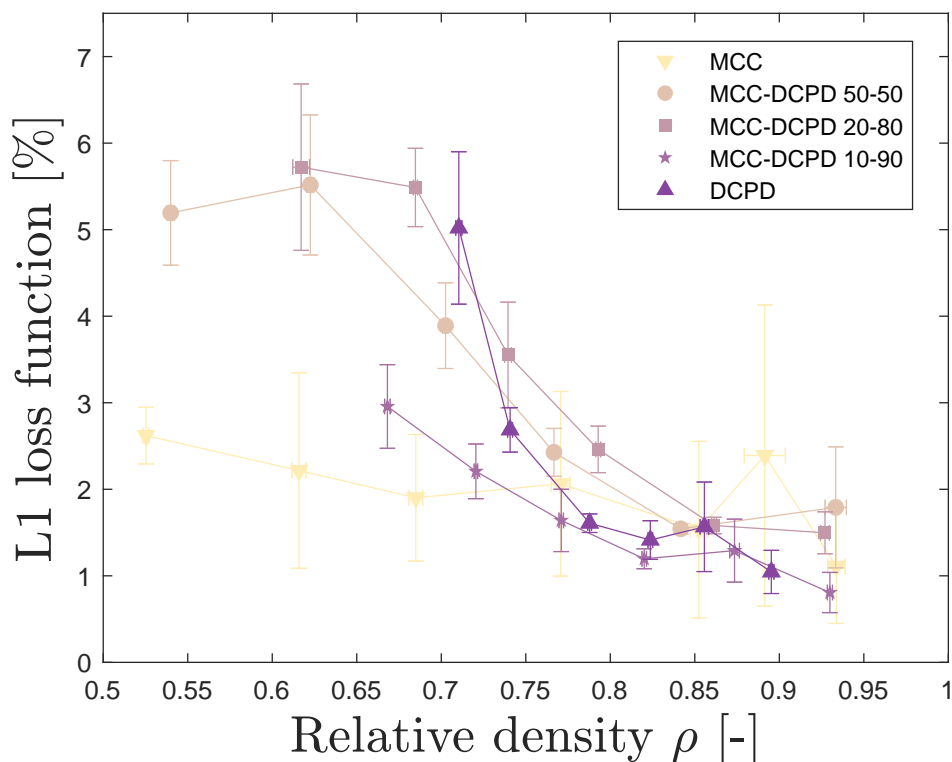


Fig. 7.2 The normalised L1 loss function underlines that FEM simulations accurately describe the experimental data with an average error between 0.5 and 5.7% when the direct parametrisation method of chapter 4 is used. For a given line segment, the L1 loss function gives the expected error of the simulated curve with respect to the experimental compaction curve. The L1 loss function of the simulated curves was computed in comparison with each experimental curve as a percentage of the peak compaction pressure. The resulting mean and standard deviation of the L1 loss function are shown here.

in chapter 6. The resulting compaction curves are shown in Fig. 7.1. Qualitatively, it can already be seen that the simulations closely follow the experimental data. The most notable deviations occur in the final stages of decompression, located at the end of the compaction curve. The decompression part of the curve start to curve backwards for the experiments whereas for the simulations the decompression remains linear. This indicates that either the mechanical properties are changing during decompression, possibly due to internal tablet failure, or that the elastic behaviour is actually nonlinear or visco-elastic. The only visible tablet failure, chipping, occurred for the 90% and 100% DCPD tablets produced with the highest compaction pressures (see section 7.1.2). External failure is therefore only present in some cases. Internal failure, such as micro-cracks, is presumed not to cause of such a significant change in the elastic modulus. Furthermore, the decompressions speed was only

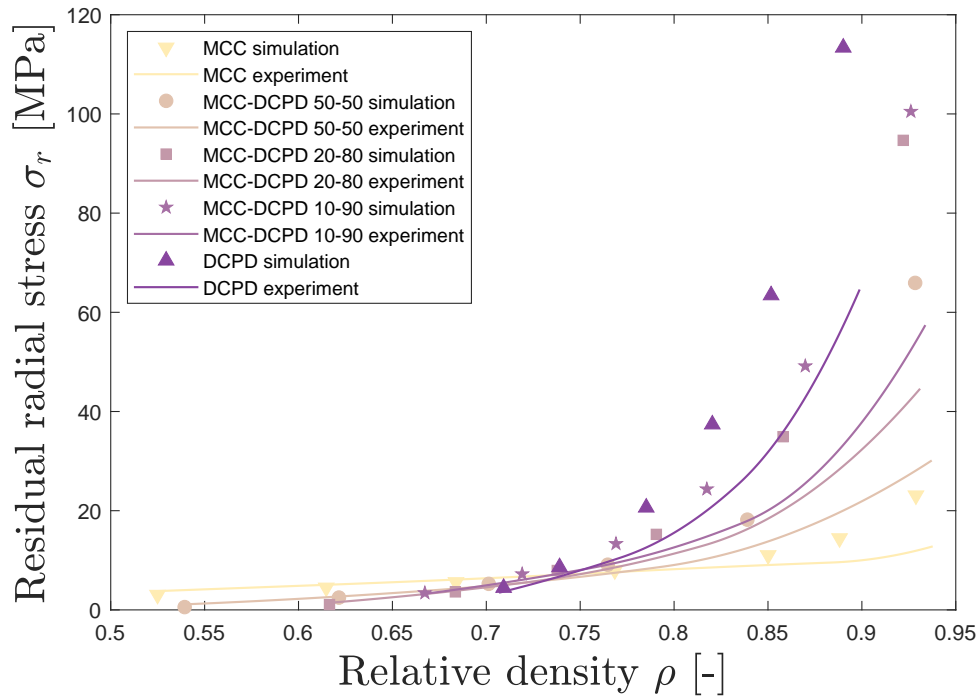


Fig. 7.3 The residual radial stress on the die wall after decompression as function of the relative density for each powder mixture. Symbols indicate predictions by the FEM simulations whereas curves indicate the experimental values. The curves are splines bound by the experimental data.

0.2 mm/s, giving quasi-static conditions. Visco-elastic is therefore also considered to be unlikely. This leaves nonlinear elastic behaviour as the most likely cause of the nonlinear decompression of the powders, as multiple authors have already suggested.[20, 21, 31, 35, 9] An inspection of the residual radial stresses after decompression further supports this. Fig. 7.3 shows that the FEM simulations have a tendency to overestimate the experimental values at high densities but are in good agreement at low densities. A nonlinear elasticity law, i.e. strain hardening, could reduce the residual radial stresses for high-density tablets and thus improve agreement with experiment.

Although the qualitative assessment shows great promise, a more quantitative assessment of the parametrisation accuracy is desirable. Therefore, the error was quantified by computing the L1 loss function (Eq. 3.3) of the simulated compaction curves with respect to the experimental curves. Fig. 7.2 shows the mean and standard deviation of the computed L1 loss functions. The inability of the simulations to describe the nonlinear unloading behaviour contributes strongly to the error. This also explains the higher errors at lower compaction densities because shorter loading paths lead to a stronger contribution of the unloading path.

The mean L1 loss function can decrease by as much as 74% if only the loading path of the curves is considered. All in all, the simulations show excellent correspondence with experiment, giving a mean error between 0.8 and 5.7% with an average of 2.5%. This validates the direct parametrisation described in chapter 4, giving an accurate representation of all materials considered without the need for user input or other *ad hoc* solutions.

Although accuracy is a basic requirement for a successful parametrisation method, a certain degree of robustness is also needed for the method to be of practical use. Therefore, the parametrisation was stress-tested by repeating the simulations with a set of parametrisations using minimal input data. Two parametrisations for DCPD were produced using, per target density, only 1 out of 10 compaction curves and 1 out of 3 radial and axial tensile strengths. One parametrisation used the samples giving the lowest maximum stresses of all, whereas the other parametrisation used the samples with the highest maximum stresses. These parametrisations, aside from using minimal data, thus also represent the extremes of the experimental data. Fig. 7.4 and 7.5 show that such parametrisations continue to closely follow the experimental data. All experimental compaction curves as well as the original parametrisation, which uses all samples, have been added to the figure for comparison. The error quantification in Fig. 7.6 further shows that the variation in the error is about equal to the experimental variability of 1 to 2%. This implies that the parametrisation is robust and that only a single observation per target density is sufficient to derive valid material properties for the FEM model.

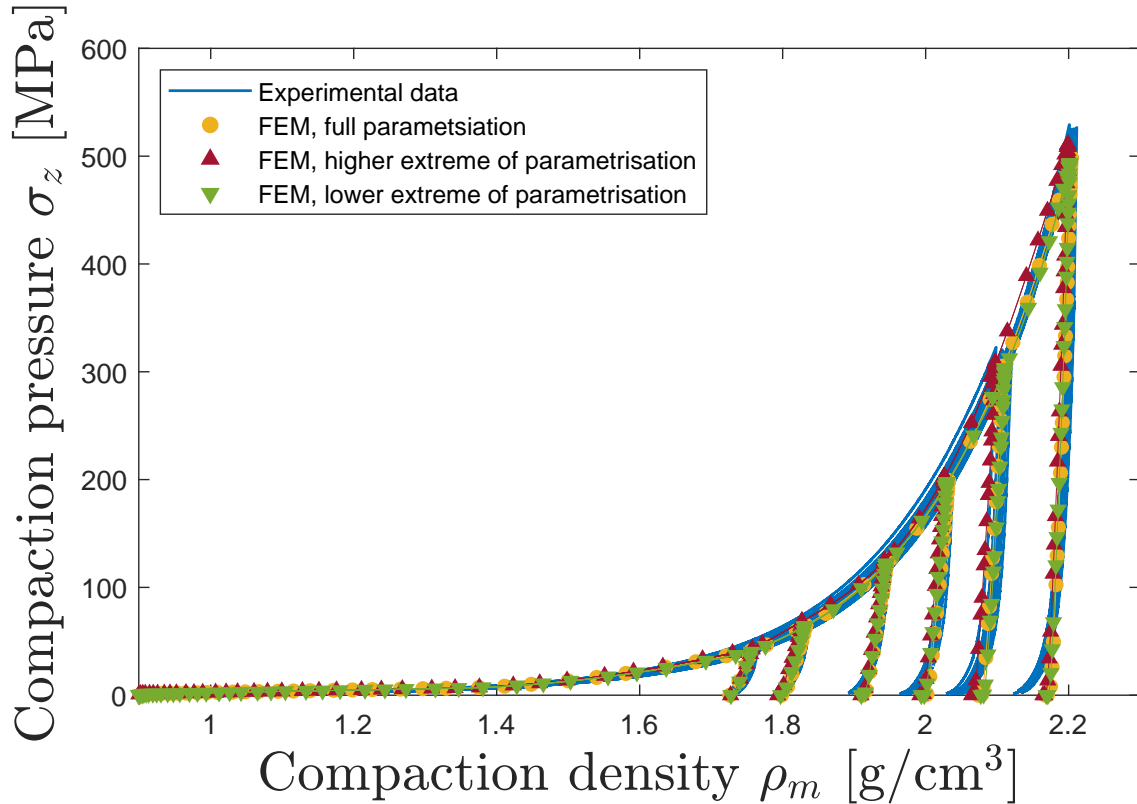


Fig. 7.4 Compaction curves are shown for the experimental data as well as various parametrizations of the FEM simulations, demonstrating that the parametrisation is stable. All compaction curves of DCPD is shown. The full parametrisation refers to a direct parametrisation in which all the data (10 curves and 3 tensile strengths per density) were used. The highest and lowest extremes of the parametrizations indicate simulations for which the direct parametrisation was done using only the data with the highest or lowest peak stress (1 curve and 1 tensile strength), respectively.

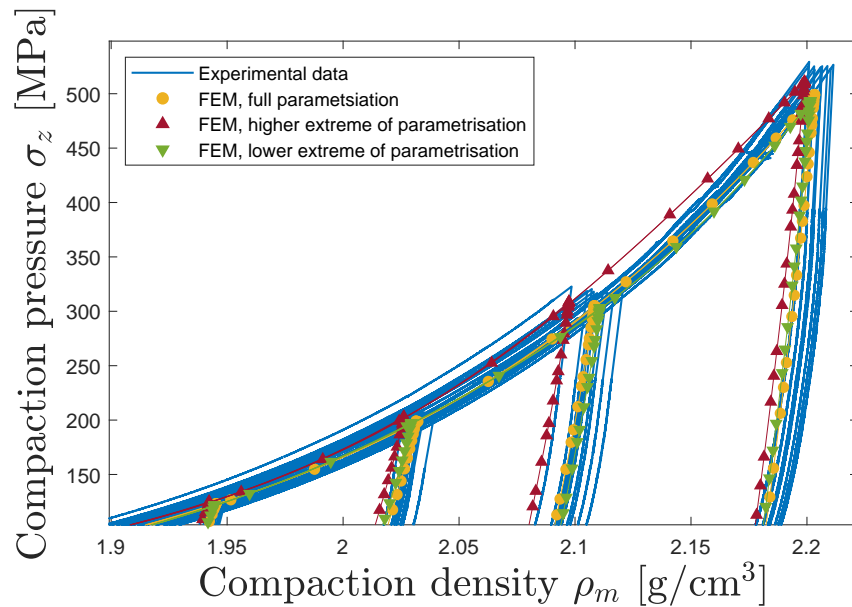


Fig. 7.5 The simulated compaction curves can be seen to stay close to the experimental compaction curves, even when the parametrisation only makes use of the 10% of data at either extreme. The data displayed is the same as in Fig. 7.4 but on a different scale.

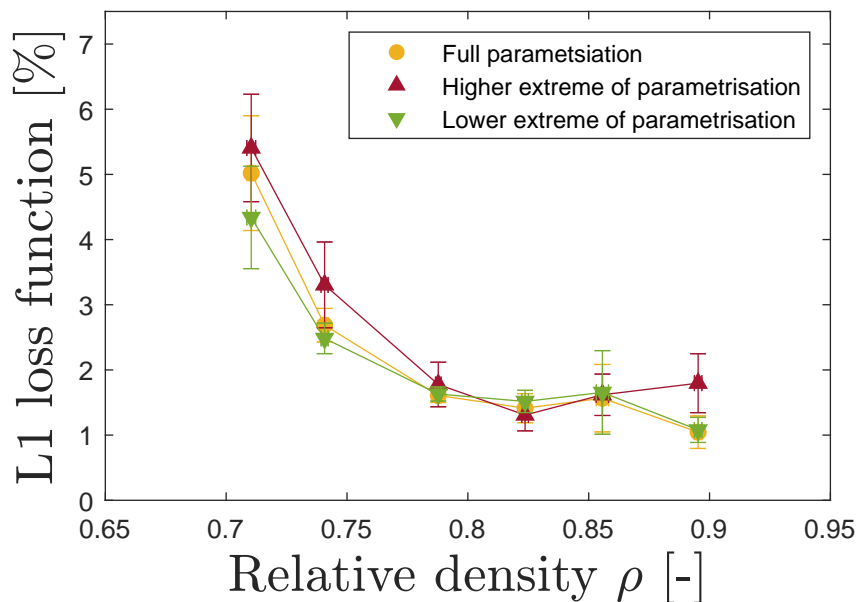


Fig. 7.6 The L1 loss function for the extremes of the parametrisation show that the variability in the parametrisation is about equal to the variability in the experimental data (1 to 2 %).

7.1.2 Qualitative identification of tablet defects

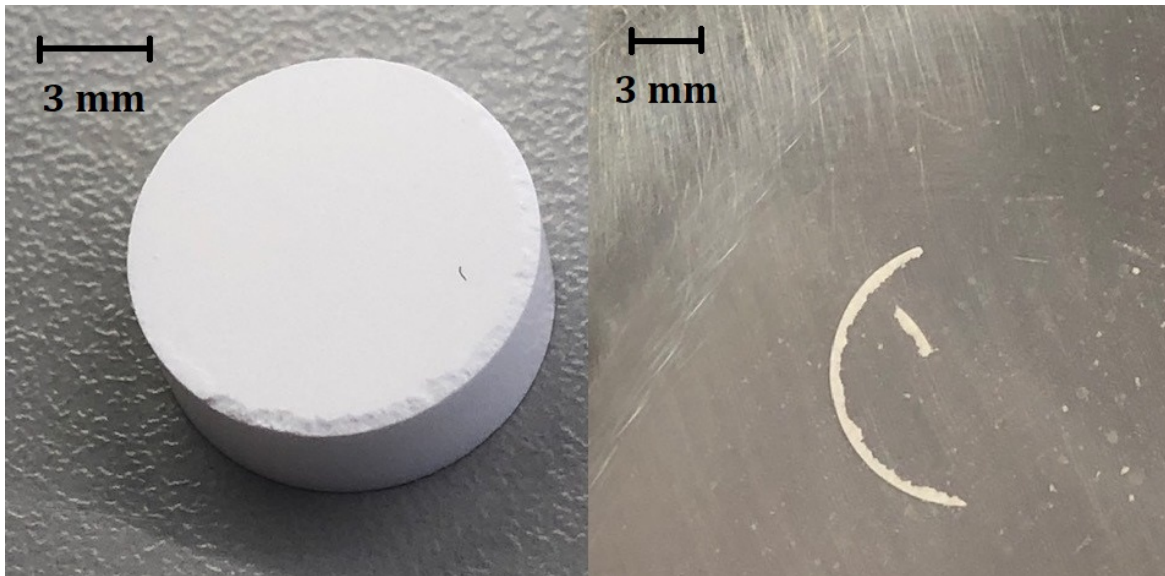


Fig. 7.7 Chipping that occurred at the lower end of the tablet upon ejection. This defect is present in the two most dense DCPD tablets and the most dense tablet with 10% MCC and 90% DCPD. The left image shows the damage on the tablet and the right image shows the trail of powder that the chipped tablet left behind. Pictures were taken with the tablets out of the die, on the lab bench.

Out of all tablet, three types of tablets showed defects. Defects were classified as chipping and could be seen at the bottom of the tablet (see Fig. 7.7). The tablets were those with 10% MCC and 90% DCPD at the highest density and the 100% DCPD at the highest two densities. Failure was expected to be most likely for these tablets because of their lower cohesions and very high compaction pressures. Inspection of the simulated shear stress profiles showed that the highest stress concentrations occur at the lower edge of the tablet. The stress concentration builds up during decompression, lowers during the start of ejection, and builds up again as the tablet approaches the die exit (see Fig. 7.8). Chipping would therefore also be expected based on the simulations. The stress patterns differ from those previously reported, possibly because the material (grade) is different and the compaction profile is double-ended instead of single-ended compaction.[15, 20, 19, 22, 23] Nonetheless, the presented model properly indicates the most likely type and location of tablet failure.

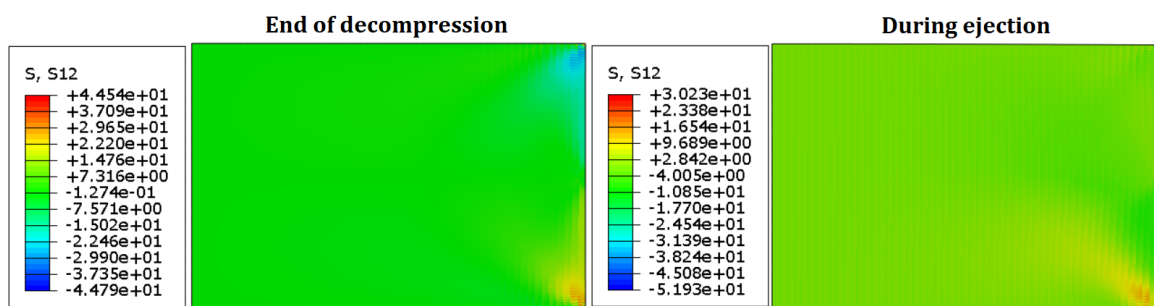


Fig. 7.8 Shear stress profiles for the most dense DCPD tablet at the end of decompression and during ejection, just before the tablet loses contact with the die wall. The high-stress regions correspond to the location where the tablet in Fig. 7.7 has chipped.

7.1.3 Evaluation of crushing simulations

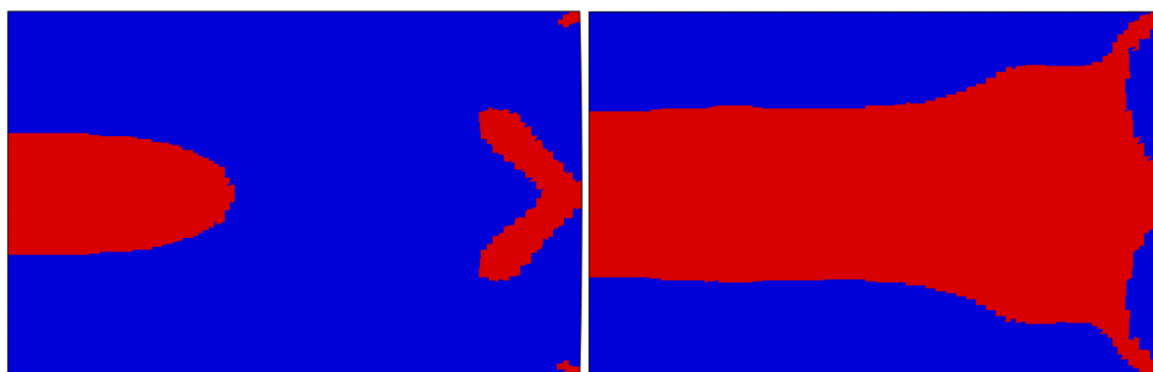


Fig. 7.9 Failure patterns of the tablet upon crushing using the AC YIELD flag in Abaqus. Red means the materials is actively yielding or undergoing plastic deformation, blue means no yield is happening. The example shown is an MCC tablet with a final relative density of 0.85.

Aside from tablet failure upon ejection, tablet failure may also occur in any of the processing steps after ejection. Tablet failure patterns resulting from external forces are therefore also of interest. Numerical crushing experiments were therefore performed in hope of being able to predict the correct failure mechanism. Furthermore, consistency can be tested by seeing if the same crushing strengths can be obtained as had been used in the parametrisation. Tablets were considered to fail if yield occurred vertically or horizontally across the entire tablet.[28] Yielding always seems to start at the tips and middle of the tablet and then arcs inwards before moving horizontally across the tablet (Fig. 7.9). In the case of denser tablets, yielding is also initiated at the centre of the tablet and propagates outwards

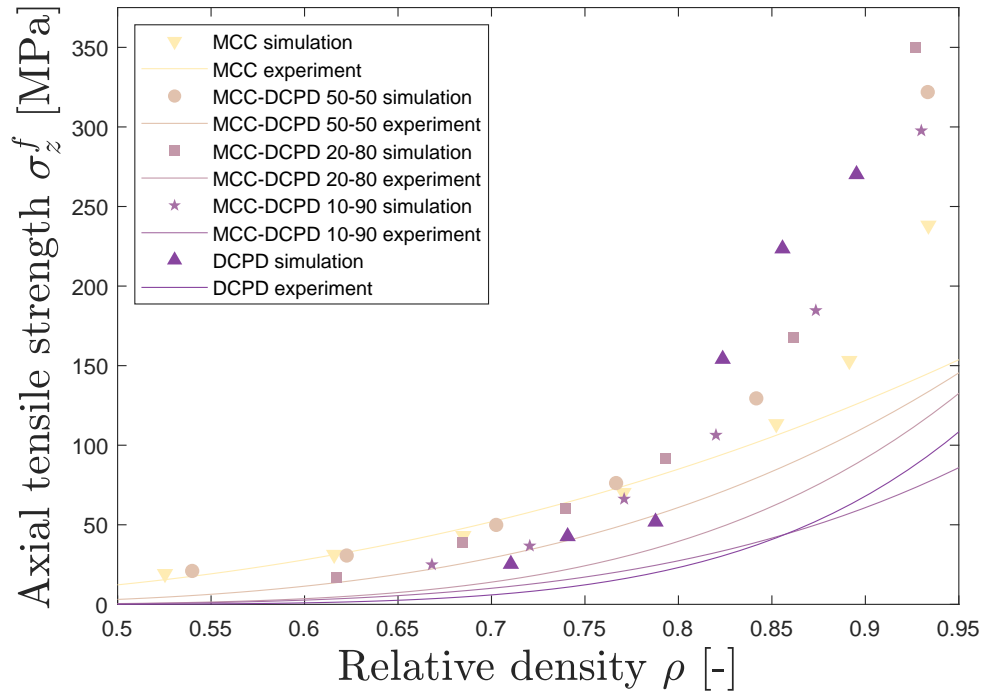


Fig. 7.10 The axial tensile strength as function of the relative density for each powder mixture. Symbols indicate predictions by the FEM simulations whereas curves indicate the experimental values. Curves are given by the fits to Eq. 3.15 and identical to those shown in Fig. 3.8.

until it connects with the yielding that initiates from the perimeter of the tablet. A more detailed look at the yield flags reveals that almost all failure happens on the cap of the DPC model. This means that the magnitude of the predicted tensile strengths depends strongly on the cap hardening curve. In fact, the tensile strengths in Fig. 7.10 seem to follow the same trend as the cap hardening curves in Fig. 4.6. Fig. 7.10 also shows that the FEM simulations have a tendency to overestimate the tensile strength of the tablet. The tensile strengths are in good agreement with experiment for low- and intermediate-density MCC tablets but strongly overestimate the tensile strengths of high-density MCC and DCPD tablets at all densities. The trends of mixture tablets are in between those observed for MCC and DCPD.

The discrepancy between the experimental and predicted tensile strengths for DCPD may result from the absence of explicit fragmentation and fracture within the model. DCPD is known to be a brittle material that fragments upon failure whereas MCC behaves more plastically.[48, 58] The dDPC parametrisation nonetheless describes the collective of all types of compressive failure within a single history-independent yield surface, i.e. the cap. However, the yield surface may be history-dependent depending on the type of compressive

failure. A second compression cycle of a frangible material would start with a fraction of the particles already being fragmented. This can reduce the internal stress dissipation within the tablet as fragmentation is a dissipation mechanism. Alternatively, it can be said that the compaction curve contains both reversible and irreversible work. Both types of work will indiscriminately contribute to the parametrised yield stress. If DCPD undergoes irreversible work due to fragmentation on the first compaction, it can thus mean that materials with more DCPD are able to absorb less irreversible work during a second compaction. This would explain why the tensile strength is more strongly overestimated for DPCD than MCC, the latter being much less frangible.[59] Moreover, irreversible work is strongly related to the amount of heat generated during compaction.[25, 36, 37] If DCPD indeed absorbs more irreversible work, this also suggests that DCPD tablets generate more heat during compression. Because the specific heat of MCC and DCPD upon heating is similar, DCPD tablets should reach higher temperatures.[60] Picker-Freyer and Schmidt showed that the surface temperature after ejection is actually lower for DCPD than MCC.[61] However, DCPD also has a higher thermal conductivity and the compression speed in the study was rather low (10 tablets per minute). It can therefore not be concluded if DCPD indeed absorbs more irreversible work and future studies on high-speed compression of DCDP and MCC are needed. Such studies can be used to test the hypothesis that irreversible work (fragmentation) is responsible for the overestimation of the yield stress in tablets. Moreover, if the hypothesis is true, such studies would also show that the yield stress (i.e. cap hardening curve) increases with compression speed because the amount of irreversible work increases due to increased friction.

7.2 Indirect parametrisation (layered)

7.2.1 Validation of the indirect layered method

Having validated the direct parametrisation method, the indirect parametrisation methods are to be validated next.

As mentioned in chapter 5, the first method was to simulate a number of tablets with different layer arrangements. This also gives an idea of the mechanical interaction between the components. The compaction curves in Fig. 7.11 show that a composite made out of two horizontally- or staircase-oriented layers mimic the behaviour of the real mixture the best. Any other spatial arrangement of the layers leads to an overestimation of the compaction pressure. The horizontal underestimates the compaction pressure near the middle of the curve. All arrangements overestimate the compaction pressure near the end. The staircase

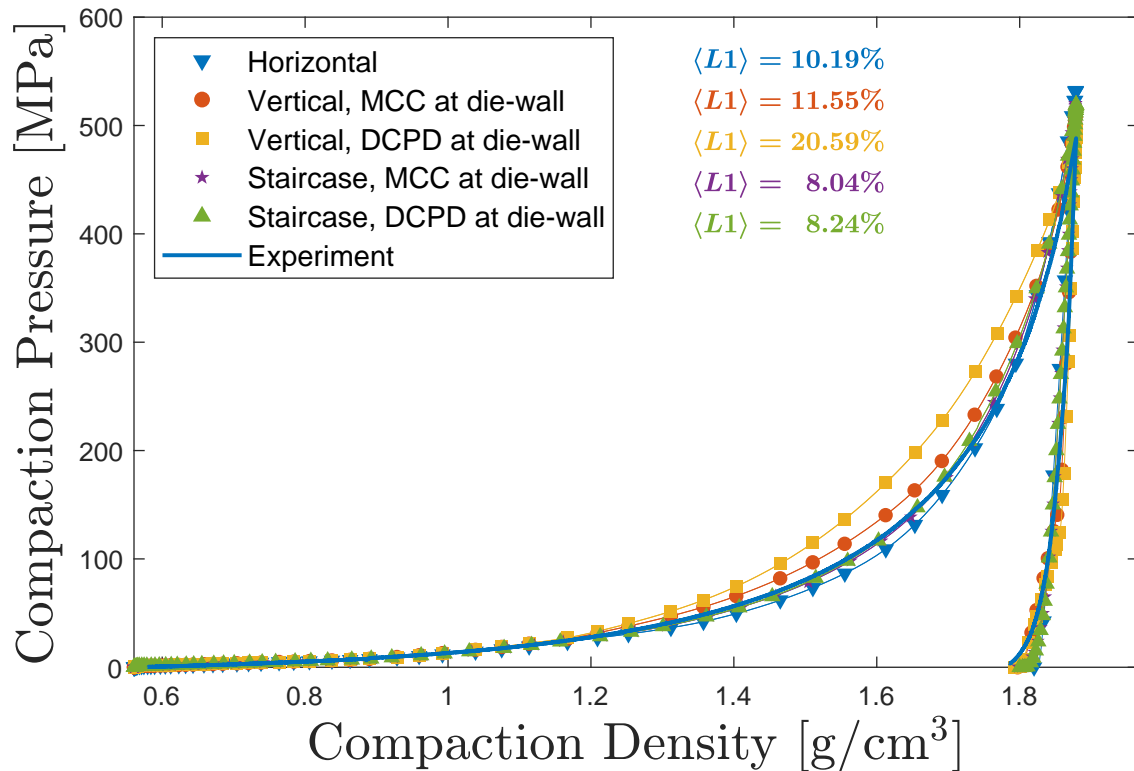


Fig. 7.11 Compaction curves resulting from the various spatial arrangements of segregated MCC and DCPD layers shown in Fig. 5.1. This was 50%-50% MCC-DCPD to the highest target density. The mean L1 loss function is also given for each arrangement. The horizontal and staircase bilayers are closest to that of the experimental homogeneous powder mixture.

arrangement seems to outperform the horizontal arrangement based on the L1 loss function. This is probably due to the staircase orientation showing a slightly nonlinear decompression path. However, the staircase orientation is more complex and the difference in performance with respect to horizontal orientation is about 2%. For simplicity, it was thus decided to continue with horizontally-oriented layers.

Simulations with horizontal layers were done for all mixtures considered. The results can be seen in Fig. 7.12 and 7.13. The L1 loss function varied from 1.4 to 14.0% with a mean of 4.5%. Given that only the data of the pure components was used for these simulations, this gives a good prediction of the compaction behaviour of the mixtures. The Reynolds et al. model can also be used, the results of which are shown in Fig. 7.14 and 7.15. The L1 loss function varied from 0.8 to 10.0% with a mean of 3.1%. This appears to be better than the FEM bilayer simulations. However, the Reynolds et al. model makes no prediction for the decompression part of the curve, which typically increases the L1 loss function.

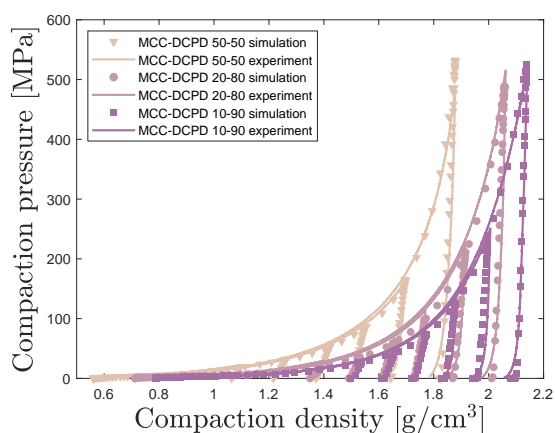


Fig. 7.12 The simulated compaction curves of tablets with horizontal bilayers.

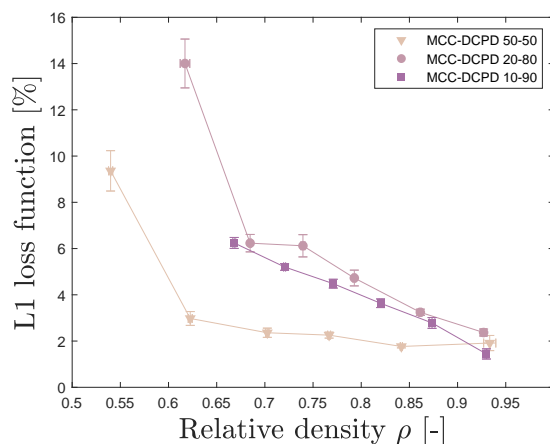


Fig. 7.13 The L1 loss function for the simulations with tablets with horizontal bilayers.

7.2.2 Implications for the mixing model

Nonetheless, the bilayer method does not give meaningful predictions of the stress distributions within a tablet because of the layer structure. It is also not possible to simulate the ejection, where failure most typically occurs, or crushing of the tablet because the layers would separate due to the absence of cohesion between the layers. The layer method can thus be used to predict the compaction behaviour of mixtures but a method that truly mixes the material properties is still preferred.

The agreement between the behaviour of the horizontally oriented composite and the homogeneous mixture implies that isostress conditions may be applicable. This would mean that the stress within each of the two materials within the powder mixture is identical, as opposed to iso-strain conditions, where the deformation is constrained to be equal. It is also noted that the DEC profile is symmetric about the middle of the powder. If both of these conditions apply, it would also mean that increasing the number of horizontal layers should not change the compaction behaviour. Note that this only holds for an even number of layers, because an odd number of layers would mean that the mass distribution of one of the two material components would shift towards the perimeter of the tablet, breaking the symmetry that also holds for a true mixture. Furthermore, flipping the tablet vertically should not change the compaction behaviour. A non-exhaustive set of simulations was done featuring multi-layered tablets. A single mesh was used but nodes were given different material properties based on the assigned layers. These simulations seem to suggest that these assertions are indeed correct, as variation in the compaction behaviour were minimal. This further implies that isostress conditions can be used to describe the compaction behaviour of multi-component mixtures.

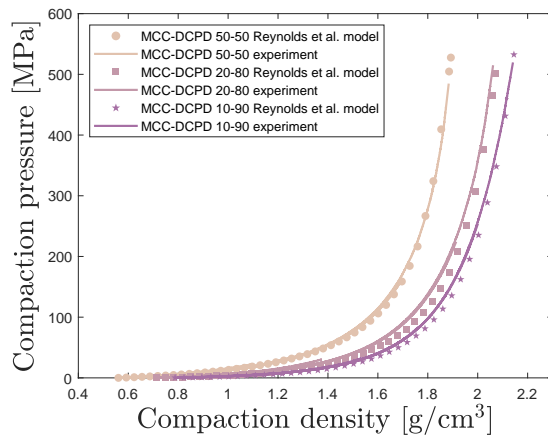


Fig. 7.14 The loading part of the compaction curves predicted by the model of Reynolds et al.[47]

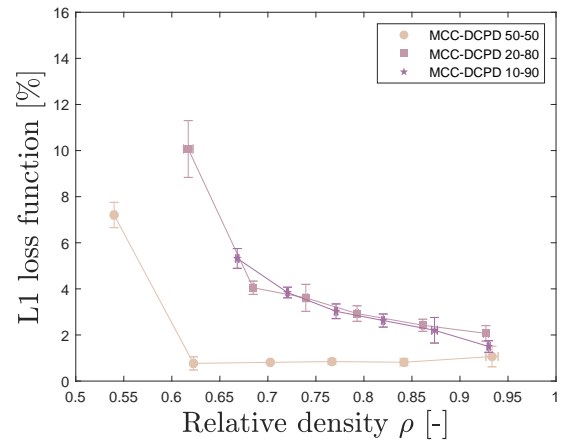


Fig. 7.15 The L1 loss function for the model of Reynolds et al.[47]

Layer arrangement:	Horizontal		Vertical		Staircase	
	MCC	DCPD	MCC	DCPD	MCC	DCPD
Material at die-wall:						
σ_z^{\max} , maximum axial stress	532	532	509	496	521	519
σ_r^{\max} , maximum radial stress	359	359	334	292	346	347
σ_r^{res} , residual radial stress	71	71	64	82	55	67
$\sigma_r^{\max}/\sigma_z^{\max}$	0.67	0.67	0.64	0.59	0.66	0.67
$\sigma_r^{\text{res}}/\sigma_z^{\max}$	0.13	0.13	0.13	0.17	0.11	0.13

Table 7.1 The maximum and residual stresses for the tablets with segregated layers of MCC and DCPD with spatial arrangements as shown in Fig. 5.1. All values are in MPa. Various stress ratios can also be seen. Arrangements with the softer material (MCC) near the perimeter of the tablet show lower ratios of residual radial to axial stress.

7.2.3 The effect of layer arrangement on the radial stress

Aside from the compaction behaviour, another noteworthy trend was observed within the various composite tablets. Changing the spatial distributions of the component materials within the composite was found to have a pronounced affect on the ratio of the residual radial stress to maximum axial stress. It appears that placing the softer material at the perimeter of the tablet lowers this ratio (Table 7.1). For example, if a tablet with two vertical (concentric) layers is considered, the ratio of the residual radial stress to maximum axial stress is lower when MCC is near the perimeter than vice-versa. The softer material can be said to cushion the pressure from the harder material on the die wall. This trend is consistent within different types of spatial arrangement (i.e. vertical layers or a staircase pattern) but not across different

spatial arrangements. The variation across different types of arrangement probably results from the large change in how the stress is distributed for different spatial arrangements. Nonetheless, these observations may be useful to reduce incidence of tablet failure in layered or multi-powder tablets as the residual radial stress has shown to be one of the strongest predictors of tableting defects.[43] Creating tablets with precise layers may be difficult in practice, but the layers do not have to be perfectly arranged as long as the softer material is placed more at the perimeter of the tablet.

The assertions mentioned in section 7.2.2 with respect to horizontal layers hold only for an even number of layers. Ideally, these assertions are also confirmed for an odd number of layers. In the case of an odd number of horizontal layers, for example in a three-layered tablet with one material in the middle and the other at the punches, the symmetry between the different layer arrangements is broken. The materials can experience different average stresses depending on which material is in the middle layer. Tablets with three horizontal layers were simulated to get an impression of how strongly this matters. Placing the softer material in the middle gives a slightly lower ratios of the maximum radial to compaction pressure (0.69 versus 0.68) and residual radial to maximum compaction pressure (0.14 versus 0.15) and a maximum compaction pressure that is 1.5% higher. This suggests that the aforementioned assertions with respect to horizontal bilayers may also hold reasonably well for an odd number of layers. However, using non-flat punches likely results in much larger differences, as the material near the punches will typically undergo much more deformation.

7.3 Indirect parametrisation (mixed)

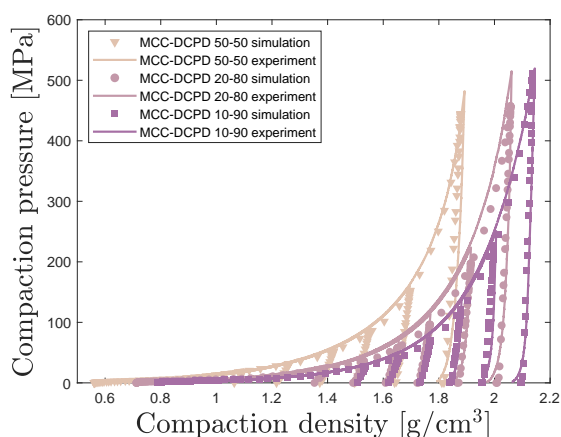


Fig. 7.16 The simulated compaction curves when using mixing rules.

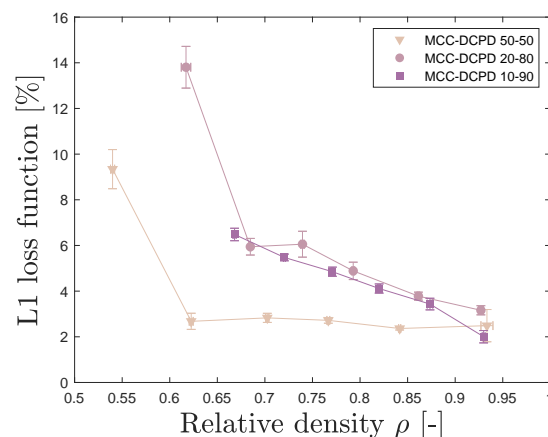


Fig. 7.17 The L1 loss function for the FEM simulations using mixing rules.

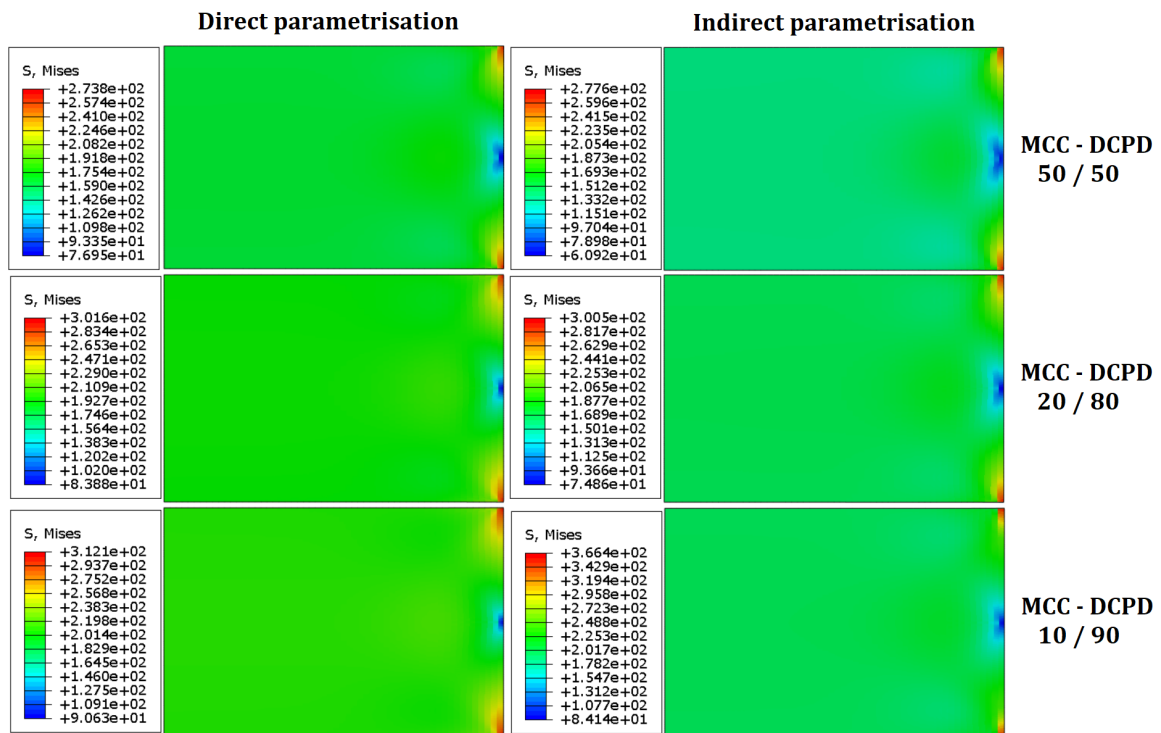


Fig. 7.18 Stress profiles at maximum compression for the direct parametrisation (left) and the indirect parametrisation (right) that uses mixing rules. The profiles show similar qualitative trends.

Following the results from section 7.2.2, a set of mixing rules were defined in chapter 5, section 5.4 using the isostress assumption. This section serves to validate these mixing rules such that, aside from the compaction profiles, stress profiles can be predicted for powder mixtures. The simulation results in Fig. 7.16 and 7.17 show that applying the mixing rules gives an accuracy similar to the layered approach. The L1 loss function varies from 2.0 to 13.8% with a mean of 4.8%, which is almost identical to the accuracy of the bilayer simulations. This validates that the proposed mixing rules can be used to predict the compaction curve of powder mixtures.

Although the mixing rules are able to predict the most essential compaction property, the motivation for using mixing rules was to obtain more detailed information about the stress distribution within mixed-powder tablets. To verify whether the mixing rules are also able to predict the correct stress profiles, the stress profiles were compared to those predicted by the direct parametrisation. Fig. 7.18 and 7.19 show a side-by-side comparison of the predicted Mises stress profiles at maximum compression and after decompression, respectively. The stress profiles resulting from the direct and indirect parametrisations produce a similar range

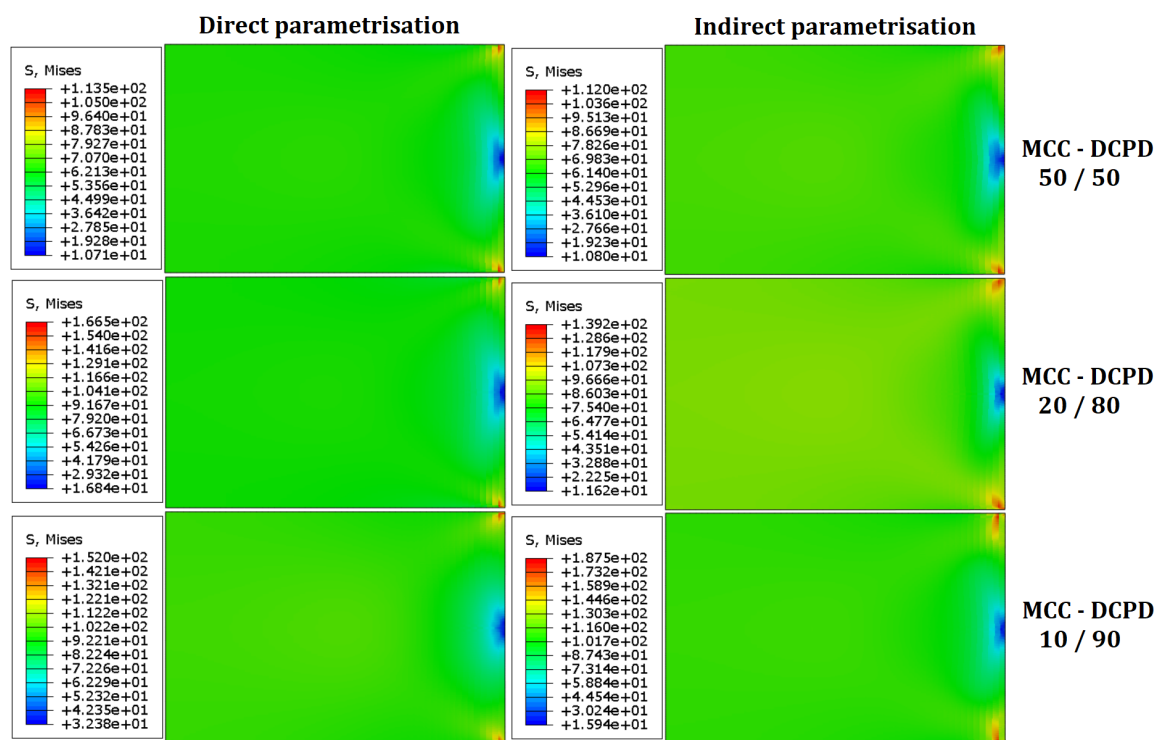


Fig. 7.19 Stress profiles after decompression for the direct parametrisation (left) and the indirect parametrisation (right) that uses mixing rules. The profiles show similar qualitative trends.

of stress values. The stress profiles themselves differ but produce the same trends as a function of tablet composition. For example, the low-stress region in the middle of the tablet near the die-wall shrinks for tablets with more DCPD. Therefore, the indirect parametrisation using mixing rules can indeed be used as a qualitative tool to assess the effect of tablet composition on the internal stresses of the tablet. Absolute values within the stress profiles should however be interpreted with caution due to their dependence on the mesh size.

Chapter 8

Conclusions and outlook

8.1 Conclusion

The overarching goal was to develop an efficient numerical methodology to predict the compaction profiles of arbitrary powder mixtures.

The first step towards this goal was parametrising the FEM model using experimental data. Powder mixtures with micro-crystalline cellulose (MCC) and dibasic calcium phosphate dihydrate (DCPD) were used as a model system. An automated work-flow, requiring minimal user input, has been developed to extract density-dependent elastic and Drucker-Prager Cap (dDPC) parameters from the experimental data. FEM simulation using this parametrisation predicted the experimental compaction curve with an expected error of 2.5% of the maximum compaction pressure, with a range from 0.8 to 5.7%. A sensitivity analysis of the parametrisation further demonstrated that the parametrisation is stable even when only a single observation is used per target density, giving a change in error that is similar to the experimental variability of 1 to 2% of the maximum compaction pressure. We therefore conclude having developed a single parametrisation method capable of describing a variety of distinct materials.

The second step towards our goal was to find out how the mixture components interact by simulating a number of powder beds with segregated layers of MCC and DCPD. Given a certain spatial arrangement of two pure powders within a single powder bed, e.g. vertical layers or a staircase pattern, the variation of that arrangement with the softer material (here MCC) closer to the die-wall appears to give a lower ratio of residual radial stress to maximum axial stress. This trend may be used to reduce the residual radial pressure, and thus the chance of defects, for layered tablets. Moreover, it was discovered that the compaction of a powder bed with strictly horizontal layers resembles the compaction of the homogeneous powder mixture with the same composition. Simulations with two horizontal layers predicted

the compaction curves of the mixtures with an expected error of 4.5% of the maximum compaction pressure with a range from 1.4 to 14.0%. The fact that horizontal layers are representative of the entire mixture suggests that the stress is isotropically distributed between the materials. This implies the existence of a representative volume element for the powder mixtures, which further implies that the stress variations caused by the difference in material properties average out at a sufficiently small length scale to justify a continuum representation of the powder. This leads to the conclusion that MCC and DCPD interact according to isostress conditions when mixed.

The final step was to construct a set of mixing rules that successfully predicts the parametrisation of a mixture using only the pure-component parametrisations. Mixing rules were defined using the aforementioned isostress condition. Elastic and dDPC parameters of the mixtures were then generated using these mixing rules and the parametrisations for pure MCC and DCPD. FEM simulations using the generated parameters predicted the compaction curves of the mixtures with an expected error of 4.8% of the maximum compaction pressure with a range from 2.0 to 13.8%. The stress distributions resulting from the different parametrisations, i.e. those using experimental data directly or those using a mixing rule, were compared. Stress distributions within the tablets were found to differ but show the same trends when changing the tablet composition. We thus conclude that the proposed mixing rules can be used to accurately predict the compaction behaviour of powder mixtures using only data of the respective pure components.

Tensile strengths and in-die residual radial stresses obtained from the FEM simulations systematically overestimate experimental values more as the DCPD content of the powder increases. Compressive yield was the dominant yielding mode at tablet failure. The overestimation of the tensile strengths was hypothesised to result from the history-independence of the compression-yield surface as the compaction curves themselves are not overestimated. It is suggested that, upon a second compression, the prior fragmentation of particles has caused a change in the location of the yield surface. This could cause an overestimation of the yield strength for tablets with a higher fraction of DCPD as DCPD is a much more brittle material than MCC.

8.2 Outlook

By far the most interesting follow-up of this study would be to validate the proposed mixing rules for ternary and quaternary mixtures. The mixing rules are defined for an arbitrary number of components, making the current methodology straightforward to extend to many-component mixtures. Nonetheless, the generalised form of the mixing rules remain to

be validated for more than two components. Furthermore, it may not be possible to get single-component compaction data for some materials. Additional rules that derive single-component parameters from a mixture, if the other component parameters are known, would therefore benefit the applicability of the mixing rules. Moreover, the mixing rules should be validated for a wider range of powder materials, as the current study only considered two types of material behaviour (plastic and brittle) as well as powders with particles of approximately equal size. A validation against particles of different shapes is also necessary. If more extensive validation of the mixing rules hold, a database of single-component experimental data could be used to predict the compaction behaviour of any resulting powder mixture.

The direct parametrisation would improve most notably by the addition of a nonlinear elasticity law. The decompression part of the compaction curve is the main source of error and shows nonlinear elastic behaviour. Furthermore, nonlinear elasticity may reduce the overestimation of the residual radial stress for high-density tablets. To avoid interference with other parts of the parametrisation and minimize additional effort, we recommend using the modified compaction experiments as suggested by Mazel et al. to parametrise nonlinear elasticity.[32]

Finally, the current parametrisation remains a continuum description and is incapable of describing some of the more nuanced physics of powder compaction. Physical phenomena that the current FEM model cannot describe are the exact moment of tablet failure (fracture), nonlinear recovery (nonlinear elasticity), and changes of the mechanical behaviour that result from changes in the dwell-time or precompression conditions (visco-elasticity). A bottom-up parametrisation of the FEM model may improve the description of these physical phenomena. For example, Gao et al. used the Discrete Element Method (DEM) to predict compaction behaviour and were able to describe the nonlinear recovery of the powder.[62] DEM can also be used to generate initial velocity distribution for FEM simulations of more dynamic problems such as roll compaction.[63] However, DEM still has difficulty to accurately describe the entire range of compaction densities because DEM neglects many-body interactions. For this reason, a number of studies used multi-particle FEM instead, where each particle is given a mesh of its own, to study powder compaction.[64–68] Two of these studies were able to derive DPC model parameters from MPFEM simulations that can then be used to do FEM simulations on a larger scale. [64, 67] Despite its successes, the computational cost of MPFEM remains prohibitively high for routine applications in industry. A promising compromise between DEM and MPFEM, both in accuracy and computation cost, may be a simulation method that applies the many-body contact laws as proposed by Gonzalez.[69]

References

- [1] Ahmad Baroutaji, Keith Bryan, Mustafa Sajjia, and Sandra Lenihan. Mechanics and Computational Modeling of Pharmaceutical Tableting Process. In *Reference Module in Materials Science and Materials Engineering*. Elsevier, Walthm, MA, USA, Jan 2017.
- [2] John C. Cunningham, Denita Winstead, and Antonios Zavaliangos. Understanding variation in roller compaction through finite element-based process modeling. *Comput. Chem. Eng.*, 34(7):1058–1071, Jul 2010.
- [3] A. Michrafy, H. Diarra, J. A. Dodds, M. Michrafy, and L. Penazzi. Analysis of strain stress state in roller compaction process. *Powder Technol.*, 208(2):417–422, Mar 2011.
- [4] Ariel R. Muliadi, James D. Litster, and Carl R. Wassgren. Validation of 3-D finite element analysis for predicting the density distribution of roll compacted pharmaceutical powder. *Powder Technol.*, 237:386–399, Mar 2013.
- [5] Alon Mazor, Lucia Perez-Gandarillas, Alain de Ryck, and Abderrahim Michrafy. Effect of roll compactor sealing system designs: A finite element analysis. *Powder Technol.*, 289:21–30, Feb 2016.
- [6] Alexander Krok and Chuan-Yu Wu. Evolutions of temperature and density during roll compaction of a pharmaceutical excipient. *Int. J. Pharm.*, 572:118822, Dec 2019.
- [7] K Hibbitt, B Karlsson, and P Sorensen. Abaqus: User’s manual: Hibbitt. *Karlsson & Sorensen*, 1988.
- [8] Structural Analysis & Simulation Software | Ansys, Jul 2021. [Online; accessed 13. Aug. 2021].
- [9] Shuji Ohsaki, Kazune Kushida, Yu Matsuda, Hideya Nakamura, and Satoru Watano. Numerical study for tableting process in consideration of compression speed. *Int. J. Pharm.*, 575:118936, Feb 2020.
- [10] J. C. Cunningham, I. C. Sinka, and A. Zavaliangos. Analysis of tablet compaction. I. Characterization of mechanical behavior of powder and powder/tooling friction. *J. Pharm. Sci.*, 93(8):2022–2039, Aug 2004.
- [11] C. Shang, I. C. Sinka, and J. Pan. Constitutive Model Calibration for Powder Compaction Using Instrumented Die Testing. *Exp. Mech.*, 52(7):903–916, Sep 2011.
- [12] Abderrahim Michrafy, D Ringenbacher, and P Tchoreloff. Modelling the compaction behaviour of powders: application to pharmaceutical powders. *Powder Technology*, 127(3):257–266, 2002.

- [13] A. Michrafy, M. S. Kadiri, and J. A. Dodds. Wall Friction and its Effects on the Density Distribution in the Compaction of Pharmaceutical Excipients. *Chem. Eng. Res. Des.*, 81(8):946–952, Sep 2003.
- [14] A. Michrafy, J. A. Dodds, and M. S. Kadiri. Wall friction in the compaction of pharmaceutical powders: measurement and effect on the density distribution. *Powder Technol.*, 148(1):53–55, Oct 2004.
- [15] C-Y Wu, OM Ruddy, AC Bentham, BC Hancock, SM Best, and JA Elliott. Modelling the mechanical behaviour of pharmaceutical powders during compaction. *Powder technology*, 152(1-3):107–117, 2005.
- [16] Tuhin Sinha, Jennifer S. Curtis, Bruno C. Hancock, and Carl Wassgren. A study on the sensitivity of Drucker–Prager Cap model parameters during the decompression phase of powder compaction simulations. *Powder Technol.*, 198(3):315–324, Mar 2010.
- [17] IC Sinka, JC Cunningham, and A Zavaliangos. The effect of wall friction in the compaction of pharmaceutical tablets with curved faces: a validation study of the drucker–prager cap model. *Powder Technology*, 133(1-3):33–43, 2003.
- [18] Tuhin Sinha, Rahul Bharadwaj, Jennifer S. Curtis, Bruno C. Hancock, and Carl Wassgren. Finite element analysis of pharmaceutical tablet compaction using a density dependent material plasticity model. *Powder Technol.*, 202(1):46–54, Aug 2010.
- [19] C-Y Wu, BC Hancock, A Mills, AC Bentham, SM Best, and JA Elliott. Numerical and experimental investigation of capping mechanisms during pharmaceutical tablet compaction. *Powder Technology*, 181(2):121–129, 2008.
- [20] LH Han, JA Elliott, AC Bentham, A Mills, GE Amidon, and BC Hancock. A modified drucker-prager cap model for die compaction simulation of pharmaceutical powders. *International Journal of Solids and Structures*, 45(10):3088–3106, 2008.
- [21] Liang Hao Han, James Elliott, Serena Best, Ruth Cameron, AC Bentham, A Mills, GE Amidon, and BC Hancock. Numerical simulation on pharmaceutical powder compaction. In *Materials Science Forum*, volume 575, pages 560–565. Trans Tech Publ, 2008.
- [22] M. S. Kadiri and A. Michrafy. The effect of punch’s shape on die compaction of pharmaceutical powders. *Powder Technol.*, 239:467–477, May 2013.
- [23] Alexander Krok, Marián Peciar, and Roman Fekete. Numerical investigation into the influence of the punch shape on the mechanical behavior of pharmaceutical powders during compaction. *Particuology*, 16:116–131, Oct 2014.
- [24] L. H. Han, P. R. Laity, R. E. Cameron, and J. A. Elliott. Density and plastic strain evaluations using small-angle X-ray scattering and finite element simulations for powder compacts of complex shape. *J. Mater. Sci.*, 46(18):5977–5990, Sep 2011.
- [25] Gerard R. Klinzing, Antonios Zavaliangos, John Cunningham, Tracey Mascaro, and Denita Winstead. Temperature and density evolution during compaction of a capsule shaped tablet. *Comput. Chem. Eng.*, 34(7):1082–1091, Jul 2010.

- [26] Chenglong Shang. *Modelling Powder Compaction and Breakage of Compacts*. PhD thesis, University of, Leicester, England, UK, May 2012.
- [27] C. Shang, I. C. Sinka, and J. Pan. Modelling of the break force of tablets under diametrical compression. *Int. J. Pharm.*, 445(1):99–107, Mar 2013.
- [28] Ryoichi Furukawa, Yuan Chen, Akio Horiguchi, Keisuke Takagaki, Junichi Nishi, Akira Konishi, Yoshiyuki Shirakawa, Masaaki Sugimoto, and Shinji Narisawa. Numerical evaluation of the capping tendency of microcrystalline cellulose tablets during a diametrical compression test. *Int. J. Pharm.*, 493(1):182–191, Sep 2015.
- [29] Vincent Mazel, Harona Diarra, Virginie Busignies, and Pierre Tchoreloff. Study of the Validity of the Three-Point Bending Test for Pharmaceutical Round Tablets Using Finite Element Method Modeling. *J. Pharm. Sci.*, 103(4):1305–1308, Apr 2014.
- [30] Vincent Mazel, Harona Diarra, Virginie Busignies, and Pierre Tchoreloff. Comparison of different failure tests for pharmaceutical tablets: Applicability of the Drucker–Prager failure criterion. *Int. J. Pharm.*, 470(1):63–69, Aug 2014.
- [31] H. Diarra, V. Mazel, A. Boillon, L. Rehault, V. Busignies, S. Bureau, and P. Tchoreloff. Finite Element Method (FEM) modeling of the powder compaction of cosmetic products: Comparison between simulated and experimental results. *Powder Technol.*, 224:233–240, Jul 2012.
- [32] Vincent Mazel, Virginie Busignies, Harona Diarra, and Pierre Tchoreloff. Measurements of Elastic Moduli of Pharmaceutical Compacts: A New Methodology Using Double Compaction on a Compaction Simulator. *J. Pharm. Sci.*, 101(6):2220–2228, Jun 2012.
- [33] H. Diarra, V. Mazel, V. Busignies, and P. Tchoreloff. Sensitivity of elastic parameters during the numerical simulation of pharmaceutical die compaction process with Drucker-Prager/Cap model. *Powder Technol.*, 332:150–157, Jun 2018.
- [34] Sean Garner, John Strong, and Antonios Zavaliangos. The extrapolation of the Drucker–Prager/Cap material parameters to low and high relative densities. *Powder Technol.*, 283:210–226, Oct 2015.
- [35] Harona Diarra, Vincent Mazel, Virginie Busignies, and Pierre Tchoreloff. FEM simulation of the die compaction of pharmaceutical products: Influence of visco-elastic phenomena and comparison with experiments. *Int. J. Pharm.*, 453(2):389–394, Sep 2013.
- [36] Antonios Zavaliangos, Steve Galen, John Cunningham, and Denita Winstead. Temperature Evolution during Compaction of Pharmaceutical Powders. *J. Pharm. Sci.*, 97(8):3291–3304, Sep 2007.
- [37] Alexander Krok, Pablo García-Triñanes, Marian Peciar, and Chuan-Yu Wu. Finite element analysis of thermomechanical behaviour of powders during tableting. *Chem. Eng. Res. Des.*, 110:141–151, Jun 2016.

- [38] V. Busignies, B. Leclerc, P. Porion, P. Evesque, G. Couarraze, and P. Tchoreloff. Investigation and modelling approach of the mechanical properties of compacts made with binary mixtures of pharmaceutical excipients. *Eur. J. Pharm. Biopharm.*, 64(1):51–65, Aug 2006.
- [39] Virginie Busignies, Pierre Evesque, Patrice Porion, Bernard Leclerc, and Pierre Tchoreloff. Mechanical properties of compacts made with binary mixtures of pharmaceutical excipients of three different kinds. *AIP Conf. Proc.*, 1145(1):240–243, Jun 2009.
- [40] Gabriele Bano, Zilong Wang, Pierantonio Facco, Fabrizio Bezzo, Massimiliano Barolo, and Marianthi Ierapetritou. A novel and systematic approach to identify the design space of pharmaceutical processes. *Comput. Chem. Eng.*, 115:309–322, Jul 2018.
- [41] Hossam M. Zawbaa, Serena Schiano, Lucia Perez-Gandarillas, Crina Grosan, A. Michrafy, and Chuan-Yu Wu. Computational intelligence modelling of pharmaceutical tableting processes using bio-inspired optimization algorithms. *Adv. Powder Technol.*, 29(12):2966–2977, Dec 2018.
- [42] Shengyun Dai, Bing Xu, Zhiqiang Zhang, Jiaqi Yu, Fen Wang, Xinyuan Shi, and Yanjiang Qiao. A compression behavior classification system of pharmaceutical powders for accelerating direct compression tablet formulation design. *Int. J. Pharm.*, 572:118742, Dec 2019.
- [43] Shubhajit Paul, Yuktेशwar Baranwal, and Yin-Chao Tseng. An insight into predictive parameters of tablet capping by machine learning and multivariate tools. *Int. J. Pharm.*, 599:120439, Apr 2021.
- [44] Ana Luiza P. Queiroz, Waleed Faisal, Ken Devine, Hazel Garvie-Cook, Sonja Vucen, and Abina M. Crean. The application of percolation threshold theory to predict compaction behaviour of pharmaceutical powder blends. *Powder Technol.*, 354:188–198, Sep 2019.
- [45] Chuan-Yu Wu, Serena M. Best, A. Craig Bentham, Bruno C. Hancock, and William Bonfield. A simple predictive model for the tensile strength of binary tablets. *Eur. J. Pharm. Sci.*, 25(2):331–336, Jun 2005.
- [46] Chuan-Yu Wu, Serena M. Best, A. Craig Bentham, Bruno C. Hancock, and William Bonfield. Predicting the Tensile Strength of Compacted Multi-Component Mixtures of Pharmaceutical Powders. *Pharm. Res.*, 23(8):1898–1905, Aug 2006.
- [47] Gavin K. Reynolds, Jacqueline I. Campbell, and Ron J. Roberts. A compressibility based model for predicting the tensile strength of directly compressed pharmaceutical powder mixtures. *Int. J. Pharm.*, 531(1):215–224, Oct 2017.
- [48] Sameh Abdel-Hamid and Gabriele Betz. Study of radial die-wall pressure changes during pharmaceutical powder compaction. *Drug Dev. Ind. Pharm.*, 37(4):387–395, Apr 2011.
- [49] Ronald Midgley Nedderman. *Statics and kinematics of granular materials*. Cambridge University Press, 2005.

- [50] Changquan (Calvin) Sun. A novel method for deriving true density of pharmaceutical solids including hydrates and water-containing powders. *J. Pharm. Sci.*, 93(3):646–653, Dec 2003.
- [51] Martin Kuentz and Hans Leuenberger. Pressure susceptibility of polymer tablets as a critical property: A modified heckel equation. *J. Pharm. Sci.*, 88(2):174–179, Feb 1999.
- [52] Eugene Ryshkewitch. Compression Strength of Porous Sintered Alumina and Zirconia. *J. Am. Ceram. Soc.*, 36(2):65–68, Feb 1953.
- [53] Lundgren J. SPLINEFIT - File Exchange - MATLAB Central, Apr 2019. [Online; accessed 28. Jul. 2021].
- [54] P. C. Carnavas and N. W. Page. Elastic properties of compacted metal powders. *J. Mater. Sci.*, 33(18):4647–4655, Sep 1998.
- [55] Susan Nachtrab. Percolation and Elasticity of Networks - From Cellular Structures to Fibre Bundles. *Friedrich-Alexander-Universität Erlangen-Nürnberg (FAU)*, 2011.
- [56] Bruno C. Hancock, Nestor Mojica, Kimberley St. John-Green, James A. Elliott, and Rahul Bharadwaj. An investigation into the kinetic (sliding) friction of some tablets and capsules. *Int. J. Pharm.*, 384(1):39–45, Jan 2010.
- [57] Helge E Krex. *Maskin ståbi*. Teknisk forlag, 1978.
- [58] C Doldan, C Souto, A Concheiro, R Martinez-Pacheco, and JL Gómez-Amoza. Dicalcium phosphate dihydrate and anhydrous dicalcium phosphate for direct compression: a comparative study. *International journal of pharmaceuticals*, 124(1):69–74, 1995.
- [59] Padma Narayan and Bruno C. Hancock. The relationship between the particle properties, mechanical behavior, and surface roughness of some pharmaceutical excipient compacts. *Mater. Sci. Eng., A*, 355(1):24–36, Aug 2003.
- [60] Jarkko Ketolainen, L'udovit Kubičár, Vlastimil Boháč, Marián Markovič, and Petteri Paronen. Thermophysical Properties of Some Pharmaceutical Excipients Compressed in Tablets. *Pharm. Res.*, 12(11):1701–1707, Nov 1995.
- [61] K. M. Picker-Freyer and A. G. Schmidt. Does temperature increase induced by tableting contribute to tablet quality? *J. Therm. Anal. Calorim.*, 77(2):531–539, Aug 2004.
- [62] Yijie Gao, Giovanni De Simone, and Maya Koorapaty. Calibration and verification of DEM parameters for the quantitative simulation of pharmaceutical powder compression process. *Powder Technol.*, 378:160–171, Jan 2021.
- [63] Alon Mazor, Luca Orefice, Abderrahim Michrafy, Alain de Ryck, and Johannes G. Khinast. A combined DEM & FEM approach for modelling roll compaction process. *Powder Technol.*, 337:3–16, Sep 2018.
- [64] Faruk Güner, Ömer Necati Cora, and Hasan Sofuoğlu. Numerical modeling of cold powder compaction using multi particle and continuum media approaches. *Powder Technol.*, 271:238–247, Feb 2015.

-
- [65] Fen Huang, Xizhong An, Yuxi Zhang, and A. B. Yu. Multi-particle FEM simulation of 2D compaction on binary Al/SiC composite powders. *Powder Technol.*, 314:39–48, Jun 2017.
- [66] B. Yohannes, M. Gonzalez, A. Abebe, O. Sprockel, F. Nikfar, S. Kiang, and A. M. Cuitiño. Discrete particle modeling and micromechanical characterization of bilayer tablet compaction. *Int. J. Pharm.*, 529(1):597–607, Aug 2017.
- [67] Peter Loidolt, Manfred H. Ulz, and Johannes Khinast. Modeling yield properties of compacted powder using a multi-particle finite element model with cohesive contacts. *Powder Technol.*, 336:426–440, Aug 2018.
- [68] Ahmet Demirtas and Jerry Klinzing. Understanding die compaction of hollow spheres using the multi-particle finite element method (MPFEM). *Powder Technol.*, Jun 2021.
- [69] Marcial Gonzalez. Generalized loading-unloading contact laws for elasto-plastic spheres with bonding strength. *J. Mech. Phys. Solids*, 122:633–656, Jan 2019.